KTH Land and Water
Resources Engineering

Dynamics of internal nutrient sources in the Baltic Sea, A comparative modelling study of the Gulf of Finland

Benoît Dessirier **Safeyeh Sofie Soltani**

October 2011

TRITA-LWR Degree Project 11:24
ISSN 1651-064X
LWR-EX-11-24

Degree Project
Division of Water Resources Engineering
Department of Land and Water Resources Engineering
Royal Institute of Technology (KTH)
SE-100 44 STOCKHOLM, Sweden
Reference should be written as: Dessirier B. & Soltani S. (2011) "Dynamics of internal nutrient sources in the Baltic Sea, A comparative modelling study of the Gulf of Finland" TRITA-LWR Degree Project 11:24, 58 pp.

À mes grand-parents,

به مادرم،
به پدرم

PREFACE

This thesis was done as a supporting investigation of the water quality dynamics in the Bay of Finland, for the EU Interreg project SEABED. For more information please visit the project's website: `www.abo.fi/huso/seabed`

The two key issues that this work addresses are:

1. What modelling approach is most robust for quantifying the effect of the internal sources of phosphorus?
2. How important is the water flow dynamics for the water quality modelling?

SWEDISH SUMMARY

Intensiv mänsklig aktivitet runt Östersjön har lett till högre utsläpp av näringsämnen (kväve och fosfor) till Östersjövattnet. Denna extra tillförsel orsakar en störning i vattenekosystemet kallat eutrofiering. Ett vanligt synligt tecken på eutrofiering är en skiftning i algpopulationen där de vanligaste algarterna efterhand ersätts med blommande cyanobakterier (blågröna alger) (Dokulil & Teubner, 2011). De senaste två årtionden har vissa områden i Östersjön under sommartid drabbats av svår algblomning (Kiirikki *et al.*, 2001).

Modellering är ett sätt att förstå och beskriva eutrofieringens inre mekanismer både begripligt och kvantitativt (Savchuk, 2000). Två aspekter behöver modelleras: vattenströmmen i vattenmassan och det biogeokemiska kretsloppet. Det första innebär att man geometriskt delar upp studieområdet och analyserar de framstående transportprocesserna. Det andra behandlar eutrofieringens biologi och kemi, detta styr t.ex. den dynamiska balansen mellan de olika algarterna, de upplösta näringsämnena och färskt organiskt avfall (detritus).

Denna studie genomfördes för Finska viken där litteraturutvalda modeller som behandlar gränsytan mellan vattnet och bottensedimenten på olika sätt samtestas. Neumann & Schernewski (2008) har implementerats som en modell som bestämmer vilka processer som sker med ett kriterium baserat på bottenvattnets syrekoncentration (som de flesta av dagens modeller). Kiirikki *et al.* (2006) testas som en ny infallsvinkel baserad på mängden färskt organiskt avfall som ligger på havsbotten. Denna studie ämnar bestämma vilken modelleringsstrategi, bland de två nämnda och kombinationer av dem, ger det bästa resultatet angående noggrannhet och robusthet. Ett speciellt intresse ges till noggrannheten att återge ett visst fenomen: det inre utsläppet av fosfater, som tidigare var bundna till järnmineraler på sedimentytan, när anoxiska förhållanden inträffar.

Vattenströmmen beskrivs i följd med ökad tidsresolution: årligen, månatligen och dagligen. De två utvalda modellerna urskiljer sig först i hur de förelägger sig när anoxiska processer sker (syrekoncentrationskriterium mot kolavfallskriterium). Sedan har de olika empiriska formuleringar för hur mycket och hur snabbt järnfosfor kan släppas. Alternativen för dessa två val korsas för att separat kunna bestämma vilket kriterium som bäst förutsäger anoxiska förhållanden och vilken empirisk fluxformulering som presterar bäst. Data samlas in från Finska mätstationer för att kunna driva modellerna med verkliga temperatur- och gränsförutsättningar. Dessa mätningar möjliggör också en jämförelse av förutsägelserna med bakgrundsvärden.

Den hydrodynamiska analysen visar att två perfekt blandade lager, som representerar ytvatten och bottenvatten, räcker för att få fram en enkel men intressant bild av verkligheten. Det visar också att enbart en daglig beskrivning av strömmen kan ge tillfredställande resultat från någon av de testade biogeokemiska modellerna. Att använda tidsmedelvärden förhindrar en bra bild av de naturliga blandeffekterna av strömmarna, vilket i sin tur är en grundförutsättning för att uppnå stabila vattenekosystem.

Komparativa körningar visar att anoxiska förhållanden förutsagda med kolavfallskriteriet ger bättre resultat än med syrekoncentrationkriteriet. Det första uppvisar också mindre känslighet till dess inre parametervärden än det sista.

Det uttryck som bäst följer järnfosforsutsläppet är det där flux korreleras med mängden fosfor i färskt organiskt avfall på havsbotten, vilket föreslogs av Kiirikki *et al.* (2006).

Denna modelleringsinsats som påbörjats i denna studie kommer att fortsätta att bedrivas i mindre skala i områden kring Finska viken samt i Ålands och Stockholms skärgårdar som en del utav SEABED projektet lett av Åbo Akademi, IVL och KTH.

ACKNOWLEDGMENTS

The authors would like to express their gratitude to their supervisor on this work Vladimir Cvetkovic for his guidance and constant care. Our thanks go to the SEABED project team members, in particular to Bijan Dargahi who supplied us with one of his hydrodynamic simulations and granted us a significant amount of his time and precious advice, to Anders Jönsson who contributed to this work from the beginning and shared his expertise in eutrophication modelling, to Johanna Mattila who followed this work and provided access to datasets as well as her expert opinion, to Prabin Paul who gave us assistance. People outside the project also offered help at KTH, we can name here Christoffer Carstens and John Juston.

Precious support about presenting and formatting research results was given by Joanne Fernlund, for which we are grateful. We appreciated very much the daily help from: Aira Saarelainen, Jerzy Buczak, Imran Ali and Caroline Karlsson.

Both authors would like to address personal thanks to Lea, Kamran and Luc.

Benoît Dessirier
Safeyeh Sofie Soltani

TABLE OF CONTENTS

LIST OF FIGURES

LIST OF TABLES

ABBREVIATIONS AND GLOSSARY

3D	Three Dimensional
A	Other Algae
anoxia	Extreme form of hypoxia or "low oxygen"
Burial	Process in which the fresh detritus is buried in the deeper layers of sediments
C	Cyanobacteria
C	Carbon
DIN	Dissolved Inorganic Nitrogen
DIP	Dissolved Inorganic Phosphorus
det	Detritus
CE-QUAL-ICM	A Multi dimensional, Water Quality Model for Surface Water
Denitrification	Process of N_2 formation in gas form due to the mineralization of nitrogen detritus in the sediments
Dissolution	Process in which oxygen is transformed from gaseous phase to aqueous phase
eutrophic	Refers to a water body with high nutrient loading, high biomass production and high oxygen demand
EFDC	Environmental Fluid Dynamics Code
Fe	Iron
GEMSS	Environmental Modeling System for Surface waters
GIS	Geographic Information System
GoF	Gulf of Finland
HYPE	HYdrological Predictions for the Environment
hypoxia	Depletion of oxygen in the water body
I	Solar radiation
IVL	Swedish Environmental Research Institute
Internal loading	Phosphate release from the sediments to the near-bottom water mostly due to the reduction of oxidized iron compounds under anoxic conditions
Iron-binding	Process in which phosphorus is bound to ferric iron in the sediments under aerobic conditions

KTH	Royal Institute of Technology (in Stockholm, Sweden)
Mineralization	Process by which organic detritus is converted into inorganic chemical species
MOM	Modular Ocean Model
Mathematica	A computational software
Monte Carlo algorithm	A multi-run procedure in which random values are selected for parameters to observe the induced results' spatter
N	Nitrogen
NH_4	Ammonium
NO_3	Nitrate
Nitrification	Process in which ammonium is transformed to nitrate in the water column
N-fixation	Biological process in which cyanobacteria takes up N_2 from the atmosphere
O, O_2	Oxygen
OSF	Overturning Stream Function
ODE	Ordinary Differential Equation
oligotrophic	Refers to a water body with low nutrient loading, low biomass production and low oxygen demand
P	Phosphorus
PO_4	Phosphate
PVGIS	Photovoltaic Geographical Information System
POM	Princeton Ocean Model
Python	A programming language
Photosynthesis	Chemical process that converts carbon dioxide into oxygen
Redfield ratio	Weight ratio of C: N: P in plankton. It can also be expressed as a molecular ratio. Redfield characterized it as approximately constant in 1958.
SMHI	Swedish Meteorological and Hydrological Institute
Settling	Process of sinking detritus in the water column
Sedimentation	Process of deposition of settling detritus on the sediments surface

T	Temperature
Transport	Motion of particles due to physical causes
USEPA	United States Environmental Protection Agency
Uptake	Nutrient consumption by algal species to sustain their growth
WASP	Water Quality Analysis Simulation Program

ABSTRACT

For decades the Baltic Sea has been subject to eutrophication due to heavy anthropogenic nutrient loads on the aquatic ecosystem. Quantitative projections of its effects require an understanding of its driving mechanisms, i.e., the hydrodynamics that are responsible for the physical transport and mixing and the biogeochemical nutrients pathways within the algal ecosystem and between the particulate and dissolved phases in the water and in the sediments.

A simple basin-scale hydrodynamic framework is set for the Gulf of Finland to test different descriptions of the biogeochemical transformations and determine the most robust modelling strategy. A recently developed criterion to determine the occurrence of anoxic events, based on the amount of fresh carbon detritus in the sediments is implemented in comparison with the classical criterion based on the oxygen concentration in the bottom water.

Time-averaging of the hydrodynamics over larger than daily intervals is proved to hinder the capture of rapid mixing events jeopardizing irremediably the water quality simulation. The new carbon based criterion for anoxia shows a better dynamic response and is less sensitive to the model's internal parameters. An internal source in the sediments correlated to the amount of fresh detritus, to represent the release of iron-bound phosphorus is confirmed as a versatile modelling assumption.

Keywords: Eutrophication models; Nutrients; Biogeochemical cycles; Hydrodynamics; Gulf of Finland; Baltic Sea

1 INTRODUCTION

1.1 The Baltic Sea

The Baltic Sea is an enclosed brackish water body in northern Europe. It covers an area of 415 266 km^2 and its catchment spreads over 14 countries with an area of 1 720 270 km^2 (Fig. 1) (HELCOM, 2002). It is connected to the North Sea by several straits between the Swedish and Danish islands (Fig. 1). Surface freshwater inflow from the surrounding catchment and deep intermittent saline inflow through the straits create a strong salinity stratification that hinders mixing between the surface and the deep water masses (Reissmann *et al.*, 2009).

The Baltic area hosts various types of human activities that have a direct impact on the marine environment, e.g., coastal industries, agriculture, fish farming and urban wastewater discharge. These are producing heavy loads of nutrients on the aquatic ecosystem (HELCOM, 2004). Extensive blue-green algae blooms in the summer time have been observed for several decades in the Baltic Sea (Fonselius, 1969). They are symptoms of a disturbance of the ecosystem known as *eutrophication*.

1.2 Eutrophication

Ansari (2010) defines eutrophication as:

> "the natural process driving the ecological succession of freshwater, estuarine, and marine ecosystems".

In the context of this study, eutrophication is the enhanced algal growth due to an enrichment of nutrients, i.e. nitrogen and phosphorus.

The state of eutrophication in a given aquatic ecosystem is categorized by the *trophic status*. The *primary production*, that is the amount of organic carbon produced by photosynthesis within one annual cycle, determines the trophic status. There are two main categories: an *oligotrophic* ecosystem is characterized by low nutrient loading, low primary production and low oxygen demand whereas a *eutrophic* water body refers to high nutrient loading, high production of biomass and high oxygen demand (Fig. 2) (Dokulil & Teubner, 2011).

Fig. 1: Map of the Baltic Sea and the associated catchment, from HELCOM (2002).

Enrichment of nutrients concentration in aquatic ecosystem enhances the primary productivity of the ecosystem (Dokulil & Teubner, 2011). The trophic status is also defined by the limiting nutrient or chlorophyll-a concentrations, or by the Secchi depth which are more easily measurable variables in comparison with the primary production (Dokulil & Teubner, 2011; OECD, 1982).

Eutrophication is qualified as *cultural* when the nutrient enrichment can be traced back to anthropogenic activities (Smith & Schindler, 2009). Potential effects of cultural eutrophication in lakes, reservoirs, rivers and coastal oceans include (Smith & Schindler, 2009; Smith, 2003):

- increase of biomass of phytoplankton and macrophyte vegetation,
- shift of bloom-forming algal species that might be toxic or inedible,
- increase of biomass of benthic and epiphytic algae,
- change in species composition of macrophyte vegetation,
- increase of biomass of consumer species,
- increase of incidence of fish kills,
- reduction in species diversity,
- reduction in harvestable fish biomass,
- decrease in water transparency,
- oxygen depletion in the water body,
- taste, odor, and drinking water treatment problems and
- decrease in perceived aesthetic value of the water body.

The anthropogenic nutrient loading phenomenon can be the consequence of a disturbance in, e.g., land-use, biogeochemical cycles, aquatic biota or climatic trends. It is qualified as either *external*, if it is directly released from a human source, or *internal*, when it emanates from a natural pool like the underlying sediments.

Nutrient loading calls for management and control. In most cases, external loading from a point source, such as sewage, is more easily remedied than from a diffuse source, e.g., runoff from agricultural land and urban areas (Thornton *et al.*, 1999). But even more problematic is the internal loading of nutrients: that is the latent release of nutrients (originated by anthropogenic loading and temporarily buried) at the sediment-water interface under anaerobic conditions (Kiirikki *et al.*, 2001).

1.3 Eutrophication models and related research

Research initiatives have examined eutrophication to understand its mechanisms and limit its harmful consequences. A constant preoccupation of researchers is to provide the policy-makers with reliable quantitative projections to set the goals in terms of environmental legislations as in Kiirikki *et al.* (2001). Simulations are one way of providing such quantitative understanding of the physical and biogeochemical processes (Savchuk, 2000).

All water quality simulation models have two common features:

- they build on a hydrodynamical model that will solve the physical transport and mixing and
- they use a model of the nutrient cycle paths, including the food web and the main chemical transformations that the nutrients can undergo, both in the water and in the sediments.

The spatial complexity can range from the fully-mixed box approach to the full 3-dimensional (3D) model. Nutrient transport studies have shown that horizontally integrated models perform well in archipelago and estuarine environments (Engqvist & Andrejev, 2003).

A major family of hydrodynamical models is derived from the Princeton Ocean Model (POM) by Blumberg and Mellor. Notable features are the sigma vertical coordinate system (i.e, vertical layers of variable thickness to follow the topography) and the turbulence model by Mellor and Yamada to compute vertical mixing (POM, 2011). This family is supported by a large community of users and includes widely

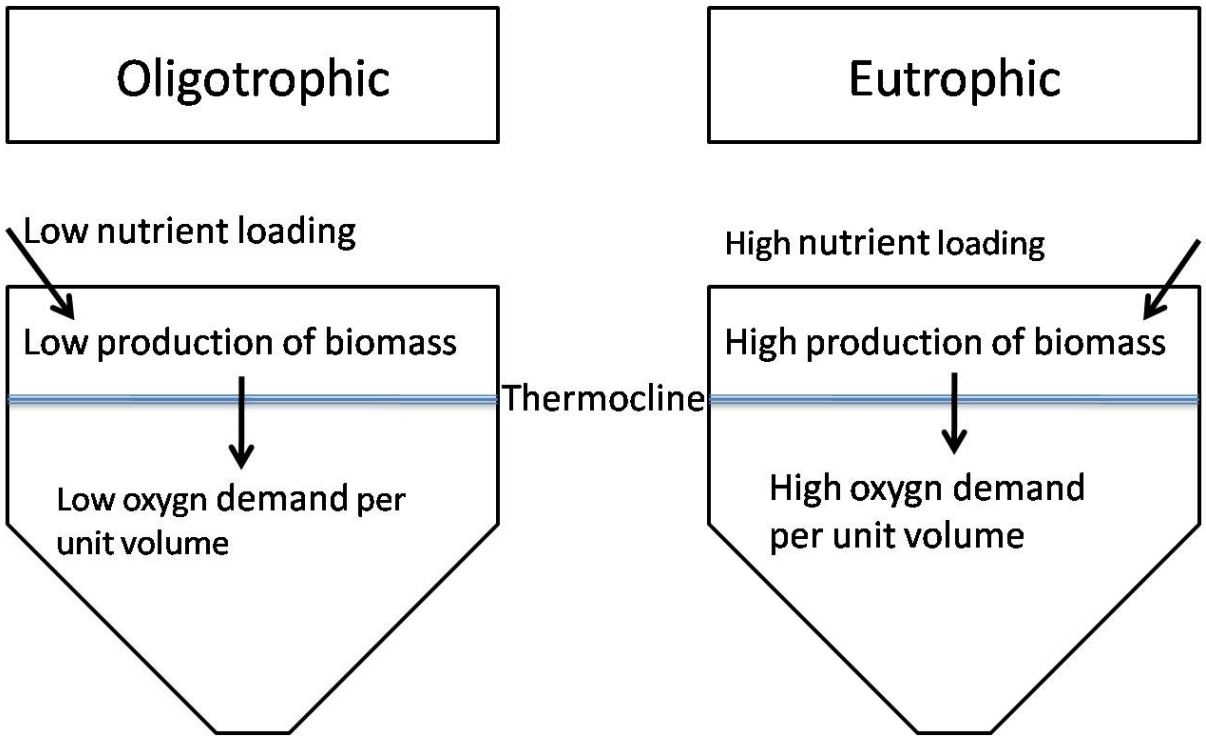

Fig. 2: Characteristics of the different trophic status, from Dokulil & Teubner (2011).

used codes like the Environmental Fluid Dynamics Code (EFDC) by the United States Environmental Protection Agency (USEPA) and the Generalized Environmental Modelling System for Surface waters (GEMSS).

Other hydrodynamical models use fixed vertical layers like the Modular Ocean Model (MOM) or the FINNFLOW model by Virtanen *et al.* (1986). GEMSS also provides that possibility.

As for nutrient cycle paths, there are two main ecosystem descriptions applied in the Baltic Sea: Stigebrandt & Wulff (1987) and Tyrrell (1999).

According to Stigebrandt & Wulff (1987), the phytoplankton is split into three different groups: diatoms as large cells species, flagellates as small cells species and cyanobacteria for the nitrogen-fixing species. Predators are gathered in a lumped zooplankton group. Dead algal material is transfered to a detritus variable, accounted in nitrogen units, which in turn becomes sediment-detritus when it reaches the sea floor. Dissolved nutrients are accounted for as either ammonium, nitrate or phosphate (Stigebrandt & Wulff, 1987; Neumann, 2000; Neumann *et al.*, 2002).

In the oceanic phytoplankton model from Tyrrell (1999), the biomass is divided into two groups: nitrogen fixing cyanobacteria and other algae. They both take up nitrogen and phosphorus from two separate pools of dissolved inorganic nutrients according to a fixed ratio first observed and introduced by Redfield (1958), further noted as the Redfield ratio.

1.3.1 Ready-to-use model packages

Ready-to-use eutrophication modelling tools like the Water Quality Analysis Simulation Program (WASP) and the Integrated Compartment Model from the CE-QUAL family (CE-QUAL-ICM) for instance are provided by the USEPA and the US army corps of engineers respectively.

WASP is aimed at receiving hydrodynamical input from the EFDC and providing managers with water quality projections to support decision-making. It offers links with Geographical Information Systems (GIS) to process the inputs and outputs. It has been used for eutrophication remediation studies in the Tampa Bay (Florida, USA) and the Potomac estuary among other cases.

CE-QUAL-ICM was initially developed as one component of a model package implemented in the Chesapeake Bay (Cerco & Cole, 1994). It was generalized and applied elsewhere after

few modifications and improvements, mostly in bays and estuaries such as the Lower Green Bay, the New York - New Jersey Harbors and Estuaries (all located in the USA).

1.3.2 *Research efforts and new modelling approaches in the Baltic Sea*

Research efforts are still conducted to improve the conceptual and numerical formulation of the processes at stake, e.g., the sediment fluxes.

Researchers at the Baltic Sea Research Institute in Warnemünde have developed a full 3D ecosystem and biogeochemical model based on the ecosystem by Stigebrandt & Wulff (1987). Their approach relies on a complete nitrogen cycle. The assumption is made that phosphorus is also present as prescribed by the Redfield ratio. The concentration of oxygen in the bottom water determines the sediment fluxes (Neumann, 2000; Neumann *et al.*, 2002). The model was later refined to include a special sediment pool grasping the action of metallic ions such as iron or manganese that can bind phosphate under oxic conditions (Neumann & Schernewski, 2008). This model is in line with the existing ready-to-use modelling packages as it calls the oxygen concentration in the water to select the occurring processes.

Finnish researchers have developed a brand new approach through a 3D ecosystem model with a high spatial resolution and long time simulations to assess the effects of nutrient load reduction scenarios in the GoF. The oceanic phytoplankton model from Tyrrell (1999) provided the basis for the ecosystem model which is built up on the top of a 3D-water quality model (Virtanen *et al.*, 1986; Koponen *et al.*, 1992). Three explicit cycles of nitrogen, phosphorous and carbon are considered. The sediment module driven by the carbon cycle simulates the release of nutrients from the sediment back to the water (Kiirikki *et al.*, 2001, 2006). This selection of the sediment processes based on the amount of fresh carbon constitutes a conceptual jump from the other approaches directly based on Oxygen.

Teams of expert were involved in regional policy-making for the Turku-Åland-Stockholm archipelago area in the frame of a project called BEVIS during 2004-2006. The goal was to coordinate local strategies to fulfill a good water quality by 2015 as required by the EU water framework directive. Two models were developed. One treated nutrients as passively transported species. The other one included transport of nutrients and the algal ecosystem described in Kiirikki *et al.* (2001). In both cases, the major shortcoming was an underestimation of the internal sources of nutrients.

A new project lead by KTH, Åbo Akademi and IVL, called SEABED, is currently conducted to reinforce the understanding of the benthic fluxes of nutrients.

1.4 Overall plan

Recent studies made it clear that internal nutrient sources in the Baltic Sea are playing a significant role in the nutrient cycling (Kiirikki *et al.*, 2006). The present work aims thus at gaining more knowledge of the dynamics of internal nutrient loading.

The plan is first to gather a global understanding of the eutrophication models. The focus is on the latest modelling alternatives for internal loading, namely Kiirikki *et al.* (2006) and Neumann & Schernewski (2008). Next comes implementing them in a common study area in the Baltic Sea. Lastly, the comparison between the two models will provide an evaluation of their performances.

The objective is to:

- determine the best modelling approach for the internal loading phenomenon.

The Gulf of Finland (GoF) was selected as study location for this master's thesis work. It is the most severe example of eutrophication in the Baltic Sea (HELCOM, 2002). The dominant longitudinal dimension of the GoF with identified inflows, outflows and stratification meet the requirements to design a box model. Lastly, connections with the Seabed Project enabled access the water quality records at the Finnish monitoring stations.

1.5 The Gulf of Finland

The Gulf of Finland (GoF) is a semi-enclosed region of the Baltic Sea, bordered by Finland to the north, Russia to the east, Estonia to the south and open to the Baltic proper to the west (Fig.3). It has a total area of approximately 30 000 km^2 and a catchment of 413 000 km^2, which gives it the particularity of having the

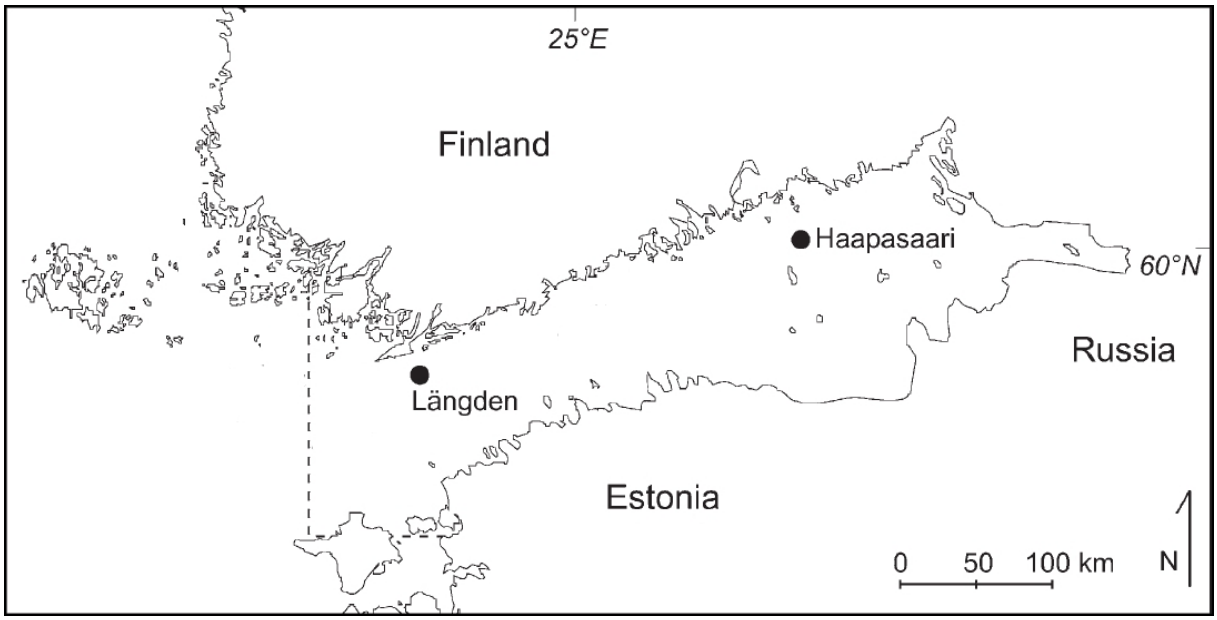

Fig. 3: Map of the Gulf of Finland (GoF) with the measuring stations Haapasaari and Längden from Kiirikki **et al.** *(2006).*

smallest ratio "area/catchment" of all the Baltic Sea basins (HELCOM, 2004; Alenius *et al.*, 1998). These physical conditions result in the GoF receiving some of the highest nutrients loadings, three times and twice the average loads in the Baltic Sea for phosphorus and nitrogen respectively (HELCOM, 2002; Schiewer, 2008).

Its main contributing river is the river Neva close to the city of Saint-Petersburg, with an average inflow of 2 500 $m^3.s^{-1}$, i.e 70% of the total freshwater inflow (SMHI, 2011). The GoF presents a clear horizontal salinity gradient between freshwater conditions at the Neva river's outlet in the east and brackish sea water conditions in the west (Schiewer, 2008). It is also subject to an unstable salinity stratification (Schiewer, 2008).

Eutrophication and algal blooms have probably always been a chronic feature of the GoF (Bianchi *et al.*, 2000). However, impacts due to anthropogenic activities have been observed since the 70's and constitute a severe issue (Schiewer, 2008). Recent policies aiming at restoring the Gulf in an oligotrophic state by cutting human releases of nutrients have shown limited response on the ecosystem. The main hypothesis is that the internal loading from the sediment is still acting as the main source of nutrients (Fonselius, 1969).

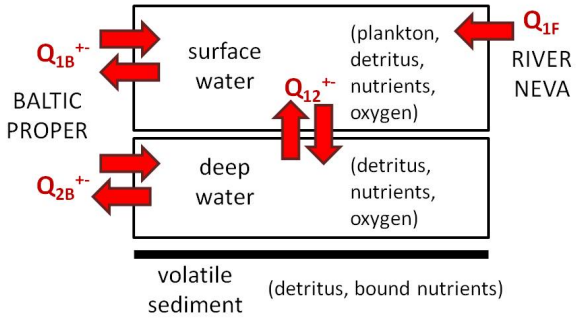

Fig. 4: Scheme of the subsystems and the flow structure.

2 METHODS

2.1 Global description

Modelling the GoF is here undertaken by the systems' approach. It consists in identifying subsystems where the processes can be described through simple formulations.

The choice here is to use fully-mixed boxes and homogeneous layers as subsystems. The GoF is divided in two boxes of water: surface and deep water, and one layer of volatile sediments (Fig.4). Each variable is characterized in a subsystem by a time-dependent ordinary differential equation (ODE).

The surface water includes all water down to 20 m deep. It is assumed to have an area $A = 30\ 000\ km^2$ (Schiewer, 2008) and a constant

height $h_1 = 20\ m$ (Kiirikki *et al.*, 2001). The surface water concentrations are thus given considering a volume $V_1 = 6\ 10^{11}\ m^3$. From a eutrophication perspective, the surface water can host plankton species, their detritus matter as well as nutrients in inorganic form and oxygen if the model requires it. Further description of the surface compartment is given in section 2.4.

The deep water encapsulates all water masses below 20 m. It was assumed for more simplicity to have the same area as the surface layer. Its height was put to $h_2 = 18\ m$ to be consistent with the average depth of the GoF: $38\ m$ (Schiewer, 2008). The corresponding volume is consequently $V_2 = 5.4\ 10^{11}\ m^3$. Regarding water quality, the deep compartment can contain dissolved inorganic nutrients, organic detritus and oxygen.

The sediment layer is an infinitely thin layer with the same area as the surface compartment (When needed to convert sediment density measurements a thickness of $10\ cm$ is assumed). It contains detritus that has reached the bottom and nutrients bound to metallic compounds like iron and manganese present in the sediments. More information about the deep water and the volatile sediments is given in section 2.5.

Exchange between the subsystems and with the exterior are accessed via hydrodynamical simulations as will be explained in section 2.3. The definition of the boundary conditions is presented in section 2.6.2.

2.2 Comparison strategy

The differences between the models are of different natures.

There is one *structural* difference: Kiirikki *et al.* considers C, N and P as three *explicit* cycles represented by different variables whereas Neumann & Schernewski considers only the cycle for N and uses the Redfield ratio to *implicitly* deduce the amount of P when it is needed. There is also an *essential* difference in the way each model prescribes if the occurring sediment processes are oxic or anoxic. Neumann & Schernewski includes an *oxygen* variable and uses it as indicator of the presence of oxygen whereas Kiirikki *et al.* uses a condition on the amount of *carbon* in the sediments to determine the nature of the occurring processes (more information is given in section 2.5). These two features are inherent to the models and cannot be changed.

There is a last *empirical* difference between the two models in the way they compute the magnitude of the internal loading flux. These two numerical formulations are interchangeable between the two models: one can pick the flux expression given by Neumann & Schernewski and apply it to an explicit system basing the sediment processes on carbon (typical of Kiirikki *et al.* (2006)) and vice versa. And it is interesting to do so to determine the distinct effects of the flux expression and the global model structure. A limit case of both flux formulations is also introduced as new expression. All three formulations are further described in section 2.5.

The focus in this study is on the internal loading. One can however only run a full system of consistent equations. To sum up, six cases are implemented in the sediment module to build the comparison (Table 1). The flow structure, the boundary conditions and the surface ecosystem dynamics however are kept constant for all runs.

2.3 Transport and Mixing

A successful implementation relies on an accurate description of the exchange between the subsystems. In this case, the inflows, outflows and the mixing between deep and surface water need to be estimated.

For the GoF, the water balance yields that precipitation and evaporation are nearly balancing each other and that the excess of freshwater inflow exits the Gulf towards the Baltic proper. Schiewer (2008) provides averaged annual estimates of the river inflow and of the inflow/outflow towards the Baltic proper (Table 2). These values correspond to the mean flow. The description of the mixing within the Gulf depends heavily on the wind conditions and displays extreme seasonal variations. That is why it is not possible to define a mean value for the vertical mixing (Reissmann *et al.*, 2009).

Two methods are now described that give more dynamic estimates of the flows.

2.3.1 The Knudsen method

The Knudsen method is a steady-state mass balance applied to an estuary. Under very simplified flow conditions, near the mouth of the entering river, the flow conditions can be de-

Table 1: Table of cases (formulations).

Formulation	Anoxic switch	P cycle	Flux expression reference	Source of P sediments	Internal P loading flux
1	O_2	implicit	Neumann & Schernewski (2008)	finite	$\frac{l_i}{h_2} I_P$
2	O_2	implicit	Kiirikki *et al.* (2006)	infinite	$\gamma_{Pin}.s_R.\frac{r_{sed}}{h_2} S$
3	O_2	implicit	present study	infinite constant rate	$\frac{l_i}{h_2} I_{P0}$
4	C	explicit	Kiirikki *et al.* (2006)	infinite	$\frac{\gamma_{Pin}}{h_2} \mu.P_V$
5	C	explicit	Neumann & Schernewski (2008)	finite	$\frac{\gamma_{Pin}}{h_2} \mu.P_{FeV}$
6	C	explicit	present study	infinite constant rate	$\frac{\gamma_{Pin}}{h_2} \mu.P_{FeV0}$

Table 2: Table of flow values.

	Schiewer (2008)	Knudsen Method	Hydrodynamic analysis (GEMSS)
Freshwater inflow ($10^9\ m^3/yr$)	114	114	121
Up/downwelling ($10^9\ m^3/yr$)	-	478 ↑	4840 ↑ 5620 ↓
Baltic Inflow ($10^9\ m^3/yr$)	480	478	1680 *surface* 690 *deep*
Baltic outflow ($10^9\ m^3/yr$)	600	593	1040 *surface* 1420 *deep*

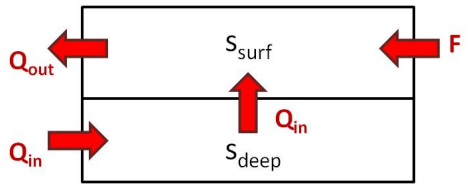

Fig. 5: Flow description for the Knudsen method: *F is the river discharge, Q_{in}: the deep inflow of saline water, Q_{out}: the surface outflow, s_{surf}: the surface water salinity and s_{deep}: the deep water salinity..*

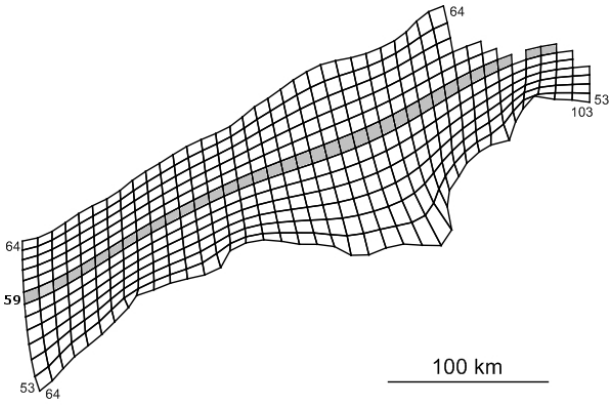

Fig. 6: Horizontal grid over the GoF for 3D calculations.

scribed as in Fig.5. A water mass balance yields:

$$Q_{in} + F = Q_{out}$$

A salt mass balance on the upper compartment yields:

$$Q_{in}.s_{deep} - Q_{out}.s_{surf} = 0$$

If the river discharge F as well as the surface and deep water salinity are measured, the inflow and the outflow are determined.

By assuming the same constant freshwater inflow as in Schiewer (2008) and by using the monthly records of salinity at the Finnish monitoring station Haapasaari (Fig.3), results close to the mean flow values are obtained for year 2004 (Table 2).

2.3.2 *Analysis of a hydrodynamic simulation*

The second method consists in using results from hydrodynamic modelling. A 3D quadrilateral grid over the Baltic Sea and a field of velocity vectors for year 2004 has been provided by B. Dargahi from the SEABED project (unpublished data). This simulation is conducted with the hydrodynamics software GEMSS mentioned in the introduction. The GoF is ex-

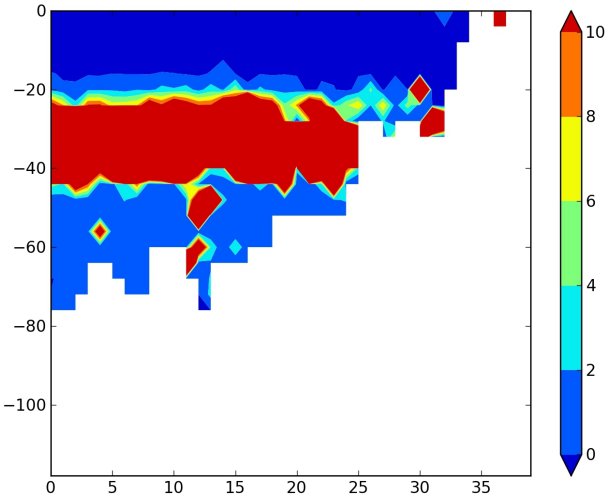

Fig. 7: Modelled Richardson gradient number along the 59^{th} West-East slice of GoF (X-axis, see indexing on Fig.6) and against the the depth in meters (Y-axis) on January the 6^{th} 2004.

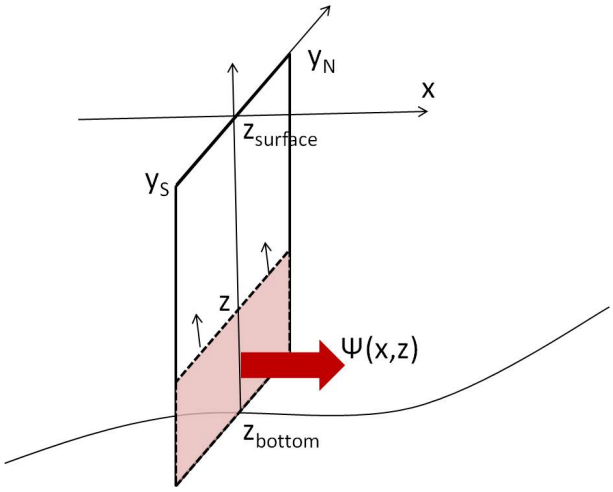

Fig. 8: Illustration of the Overturning stream function spatial summation.

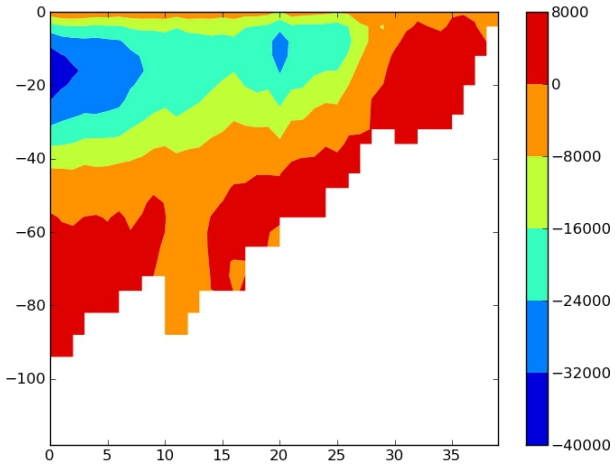

Fig. 9: Time-averaged (year 2004) zonal OSF, the unit of the OSF is m^3/s, positive (resp. negative) values show anti-clockwise (resp. clockwise) motion.

tracted from the global simulation (Fig.6). The horizontal grid size over the GoF is of approximatively 10 km and the vertical spacing is 4 m above 80 m depth and 6 m below. The time resolution is 2 $days$.

The *Richardson gradient number*, R_i is defined as:

$$R_i = -\frac{g}{\rho}\frac{\partial\rho/\partial z}{(\partial v/\partial z)^2}$$

where g is the gravity acceleration, ρ is the water density (function of salinity and temperature), $\partial\rho/\partial z$ is the density vertical gradient and $\partial v/\partial z$ is the velocity vertical gradient. It can be interpreted as the ratio between the stabilizing forces of buoyancy and the destabilizing action of the velocity variations. It gives a quantitative estimate of the mixing intensity. $R_i < 0$ means the flow is unstable and the mixing will be very high. If $R_i > 10$, the flow is stratified and very little dispersive mixing is happening.

The choice is made to model the flows like pure advective fluxes. The diffusion and dispersion effects are neglected when estimating the exchange between boxes. The delineation between the two boxes is drawn at a depth where $R_i > 10$ to ensure that advective fluxes are dominant over diffusive fluxes. This criteria is met for the analyzed slices of the GoF at a depth of 30 m (Fig.7). The flows represented on Fig.4 are thus aggregated for a divide between surface and deep water located at 30 m of depth. The obtained values are given in Table 2.

The flow values for 2004 are repeated periodically to run the simulation for several years.

The *overturning stream function* (OSF) is a flow investigation tool presented in Döös *et al.* (2004) that provides coast-to-coast aggregated values. The *time-averaged zonal OSF*, for instance, is defined as a meridional —South-North— integration (Fig.8):

$$\psi(x,z) = \frac{1}{t_1 - t_0}\int_{t_0}^{t_1}\int_{y_S}^{y_N}\int_{z_{bottom}}^{z} v_x(x,y,z)\mathrm{d}z\mathrm{d}y\mathrm{d}t$$

It gives the time-averaged cumulative volumetric flow —from bottom to surface— through a vertical —South-North— plane. The OSF is thus expressed in m^3/s. Graphically, given an

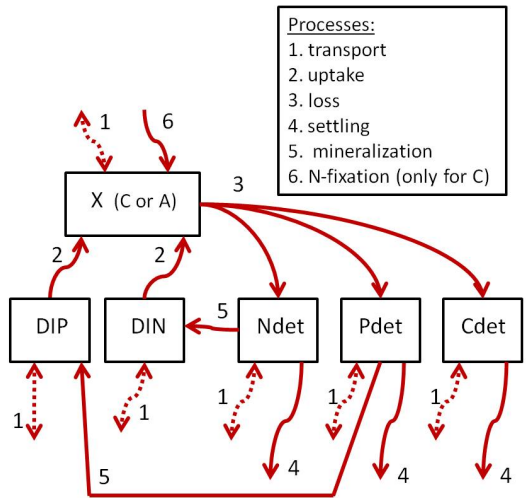

Fig. 10: Scheme of the Kiirikki* et al. *(2001) ecosystem.

upwards vertical axis and a horizontal axis directed to the right, a positive pole of the OSF indicates anti-clockwise circulation and a negative pole, clockwise. Fig.9 shows the time-averaged OSF along the longitudinal dimension of the GoF (integration in the lateral dimension). The overall circulation is qualitatively consistent with the flow values obtained from the hydrodynamic analysis: water is entering the Gulf at the surface and exiting at middle depths (Fig.9).

2.4 Ecosystem module

2.4.1 *Common ecosystem from Kiirikki* et al. *(2001)*

Short description

The ecosystem model is based on the oceanic phytoplankton model (Tyrrell, 1999) as implemented in Kiirikki *et al.* (2001). It helps to assess the effect of nutrient load reductions in the GoF. Biomass is divided into two families of phytoplankton species in competition: cyanobacteria (c_C) and other algae (c_A), both expressed as wet weight of biomass per area. They take up inorganic dissolved nutrient according to the Redfield ratio, noted as s_R (Redfield, 1958) (Fig.10). The other algae group grows faster; however, in absence of dissolved inorganic nitrogen (DIN), the N-fixing capability of cyanobacteria grants them an advantage. Dead biomass is transformed into carbon (C), nitrogen (N) and phosphorous (P) detritus according to the Redfield ratio (41:7.2:1 by weight). They are treated as variables C_{det}, N_{det}, P_{det} in the system and settle down to the deep water layer with a sinking velocity $s = 1\ m/day$. They are mineralized during settling to form DIN and DIP to the water column (Fig.10).

Detailed description

(Note from the authors: *This part, as well as the other bearing the same name, can be skipped without altering the conceptual understanding of the thesis.*)

Let X stand either for A, other algae or C, cyanobacteria. The algal growth rate (μ_X) depends on nutrient availability (DIN & DIP), solar radiation (I) and temperature (T). The nutrient limiting factors (f_{XDIN} and f_{XDIP}) and solar radiation limiting factor (f_{XI}) are calculated with the use of Michaelis-Menten kinetics. Let Y be DIN or DIP, for the nutrient limitation or I, for the solar radiation. The limiting factor is given by the following function:

$$f_{XY} = \frac{Y}{Y + K_{XY}}$$

K_{XY} values are obtained from calibration in Kiirikki *et al.* (2001). Lighting is limited during the ice cover periods within the factor f_{XI} by reducing the available radiation I. The temperature limitation function ($f_{XT\mu}$) is determined by Frisk (1982) under the form:

$$f_{XT\mu} = \exp(\int_{T_{opt\mu X}}^{T} \ln(\Theta) \mathrm{d}T)$$

where

$$\Theta = a_{T\mu X} + (1 - a_{T\mu X}) \frac{T}{T_{opt\mu X}}$$

Finally, a self shading limiting factor(f_{AC}) is considered when the area is fully covered with biomass by defining a maximum total biomass of algae (A_{max}):

$$f_{AC} = 1 - \frac{c_A + c_C}{A_{max}}$$

The full growth rate for the algal group X is the product:

$$\mu_X = \mu_{Xmax} \cdot f_{XDIN} \cdot f_{XDIP} \cdot f_{XI} \cdot f_{XT} \cdot f_{AC}$$

Losses of biomass happen at a temperature dependent rate R. C_{min} and A_{min} are minimum biomass of cyanobacteria and minimum

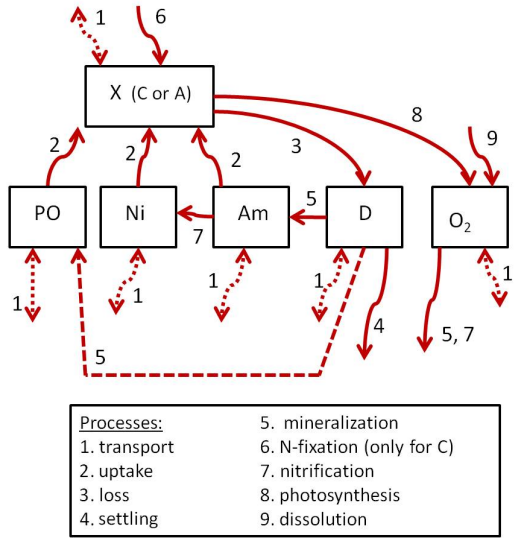

Fig. 11: Scheme of the Kiirikki* et al. *(2001) ecosystem adapted to be coupled to the sediment module from Neumann & Schernewski (2008).

biomass of algae, respectively to avoid extinction of biomass during wintertime obtained from calibration in Kiirikki *et al.* (2001):

$$R_X = R_{Xmax}.f_{XTR}.\frac{c_X - X_{min}}{c_X}$$

$$f_{XTR} = \exp(\int_{T_{optRX}}^{T} \ln(\Theta)\mathrm{d}T)$$

where

$$\Theta = a_{TRX} + (1 - a_{TRX})\frac{T}{T_{optRX}}$$

N_{det} and P_{det} are mineralized in the water column at a temperature-dependent rate of β and γ, respectively. β_0, i e. the maximal nitrogen mineralization rate is almost half of maximal phosphorous mineralization (γ_0). The current mineralization rate is given by a function of the same type as $f_{XT\mu}$ where the constants T_{optT} and a_T are replaced by $T_{opt\beta}$ (resp. $T_{opt\gamma}$) and a_β (resp. a_γ) (Garber, 1984), which yields:

$$\beta = \beta_0.f_{T\beta}(T)$$

$$\gamma = \gamma_0.f_{T\gamma}(T)$$

2.4.2 *Linkage to Neumann & Schernewski (2008)*

Short description

Dissolved inorganic nutrients species in Neumann & Schernewski (2008), are split with more complexity as Ammonium A_m (NH_4), Nitrate N_i (NO_3) and Phosphate PO (PO_4). To use the same ecosystem definition, adjustments are made. The sum of A_m and N_i is used by definition where DIN appears. The assumption is made that A_m and N_i are taken up proportionally (the ratio $\frac{A_m}{N_i}$ is the same before and after the uptake). PO is by definition the direct equivalent to DIP. Only one detritus group D is considered which is equivalent to N_{det}. An oxygen variable O_2 is also necessary to drive the model (Fig. 11). The equivalents between the two models are summarized in Table 3.

Table 3: Table of equivalence for variables.

Kiirikki *et al.* (2006)	Neumann & Schernewski (2008)
DIN	$A_m + N_i$
DIP	PO
N_{det}	D
P_{det}	$s_R.D$
N_V	S
P_V	$s_R.S$
P_{FeV}	I_P

Nutrients can undergo *mineralization* or *nitrification*. Oxygen is consumed in both processes, produced by algal photosynthesis and dissolved from the atmosphere at the sea surface (Fig. 11).

Detailed description

Mineralization transforms Detritus into Ammonium according to a rate (Neumann *et al.*, 2002):

$$L_{DA} = l_{DA}.(1 + \beta_{DA}\frac{T^2}{T^2 + T_{DA}^2})$$

A proportional amount of phosphorus is transfered into PO with the rate $s_R.L_{DA}$, where s_R is the Redfield ratio. Nitrification turns ammonium into nitrate according to a rate (Neumann *et al.*, 2002):

$$L_{AN} = \theta(O_2)\frac{O_2}{O_2 + O_{AN}}l_{AN}\exp(\beta_{AN}T)$$

In the event of oxygen depletion, nitrates can act as oxygen providers to sustain the detritus mineralization, thus creating a denitrification flux leaving the nitrate pool, expressed as: $-s_1.L_{DA}.D$. Detritus settles to the sediment

Table 4: Table of equivalence for rates.

Kiirikki *et al.* (2006)	Neumann & Schernewski (2008)
β	L_{DA}
γ	L_{DA}
s	l_{DS}
fr_P	F_r
fr_{dn}	$L_{S-denit}$
μ	r_{sed}
$\mu.\gamma_{Pin}$	l_i

layer with a constant sinking velocity l_{DS}, creating a flux: $\frac{l_{DS}}{h_1}.D$ down towards the deep waters. The equivalent rates for corresponding fluxes are summarized in Table 4.

Oxygen is produced by both algal groups, the production is estimated as:

$$\frac{s_2.A_m + s_3.N_i}{A_m + N_i}.\frac{\mu_C.c_C + \mu_A.c_A}{h_1}$$

Oxygen is consumed through nitrification and mineralization creating two respective fluxes

$$s_4.L_{AN}.A_m \text{ and}$$

$$s_2.L_{DA}.D$$

.

2.5 Deep water and Sediment module

For both configurations that are presented here, the assumption is made that no resuspension event occurs, which is verified for low near-bottom flow velocities.

2.5.1 *Neumann* et al.*'s description*

Short description

The sediment part of the cycle as described in Neumann (2000); Neumann *et al.* (2002) and Neumann & Schernewski (2008), is driven by the concentration of oxygen O_2 in the bottom water. The original 3D model considers that processes become anoxic when oxygen is locally depleted, i.e $O_2 < 0$. This criteria is not appropriate for a coarse box approach where the local bottom concentration is not available, only the whole deep water as a whole. Instead, the shift is approximated here by a higher threshold value of oxygen concentration in the deep water that denotes depletion at the sediment interface. Satisfactory results are obtained for a threshold value $O_{2T} = 8.5\ g/m^3$. Moreover,

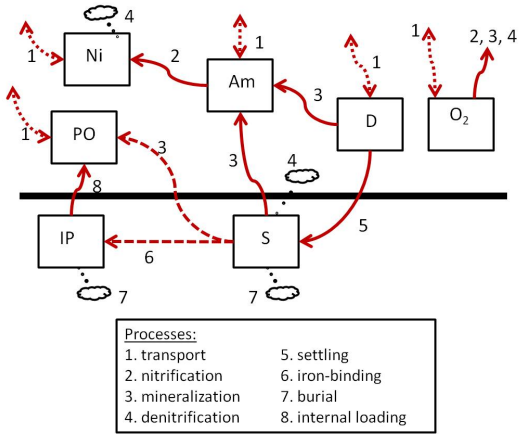

Fig. 12: Scheme of the Neumann & Schernewski (2009) water-sediment processes.

diffusive transport evens out steep gradients if the oxygen demand that causes them disappears. Another adjustment is thus tried involving the time derivative of the oxygen concentration as well. Anoxic conditions are then the combination of:

$$\begin{cases} O_2 < 8.5\ g/m^3 \\ \frac{\partial O_2}{\partial t} < 0. \end{cases}$$

The condition that yields the best results is kept for each run: threshold on O_2 only or both on O_2 and the derivative.

The deep water nutrients consist of four species. Inorganic nitrogen can take two forms: ammonium A_m or nitrate N_i, the sum of the two becoming by definition the equivalent of DIN in Kiirikki *et al.* (2001) (Fig.12). Inorganic phosphorus is accounted for as phosphate PO, the equivalent of DIP. Organic nutrients are represented by a single nitrogen detritus variable, D. The assumption is made that phosphorus detritus is present in the system according to the Redfield ratio, that is $N : P = 7.2 : 1$ (in mass). A last variable, O_2 is used for oxygen. All these species are transported according to the flow structure described in section 2.3 (Fig.12).

Processes in the deep water are *nitrification* and *mineralization*. They are quantified with the same formula as in section 2.4.2, but using here the temperature of the deep water.

The sediments belong to two variables, S and I_P. S is the nitrogen detritus that has reached the bottom. Here again the assumption is made that the corresponding amount of phosphorus is present according to the Redfield ratio. I_P is

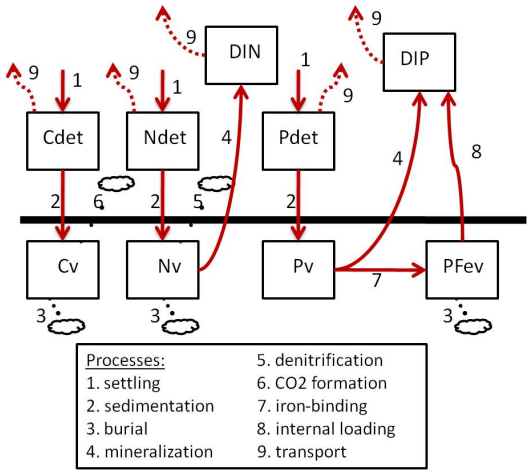

Fig. 13: Scheme of the Kiirikki* et al. *(2006) water-sediment processes.

a special variable for phosphorus that binds to iron ions when the sediments are oxygenated. It gradually releases the trapped phosphorus when the sediments are anoxic, producing the internal loading phenomenon (Fig. 12).

Three numerical formulations of the internal loading are tried in this thesis work. Formulation (1) is the direct implementation of Neumann & Schernewski (2009)'s hypothesis. Formulation (2) is conceptually derived from Kiirikki *et al.* (2006). Formulation (3) is a variation of (1) that originates from this work. The numerical expressions of each formulation is given in the detailed description.

Detailed description

Detritus settles to the sediment layer with a constant sinking velocity l_{DS}, creating a flux:

$$\frac{l_{DS}}{h_2}.D$$

from D to S. Mineralization of nitrous sediments occurs with a rate:

$$r_{sed} = r_{sed0}.\exp(\beta_{sed}.T)$$

A similar flux of phosphorus $s_R.r_{sed}.S$ leaves the sediment detritus, of which a fraction $F_r = f_{r0}.\theta(O_2)$ feeds the I_P sediment pool and the rest is released back to the dissolved phosphate PO. Under oxic conditions, nitrogen leaves the system from the detritus sediment through denitrification with a rate: $L_{S-denit} = \theta(O_2).r_{sed}$.

Another sink of nutrients is the burial that takes place from both sediment pools with a constant rate τ.

Under anoxic events, the iron-bound phosphate is liberated back to water with a rate $l_i = l_{i0}.\theta(-O_2)$ creating a flux:

$$\frac{l_i}{h_2}.I_P \qquad (1)$$

This original formulation from Neumann & Schernewski (2009) constitutes a finite source of phosphorus unlike the formulation given by Kiirikki *et al.* (2006). That is why two alternative formulations will also be investigated. In a second time, a similar formulation as in Kiirikki *et al.* (2006) is tested, that is a flux expressed as:

$$\gamma_{Pin}.s_R.\frac{r_{sed}}{h_2}.S \qquad (2)$$

In a third time, I_P is frozen as a constant I_{P0} to produce an infinite source with a flux:

$$\frac{l_i}{h_2}.I_{P0} \qquad (3)$$

Oxygen is consumed through nitrification and mineralization creating two respective fluxes Neumann *et al.* (2002):

$$s_4.(L_{AN}.A_m + \frac{r_{sed}}{h_2}.S) \text{ and}$$

$$s_2.(L_{DA}.D + \frac{r_{sed}}{h_2}.S)$$

2.5.2 *Kiirikki* et al.*'s description*

Short description

The other formulation for the sediment module is based on the sediment processes' description proposed by Kiirikki *et al.* (2006). A well oxygenated sediment surface retains nutrients. They are, however, released back to the water if anaerobic conditions prevail. In this approach the sediment nutrient cycling is driven by the settled organic matter, instead of the near-bottom oxygen concentration. Oxidization of organic carbon (C) to CO_2 depletes the oxygen in the sediments while the near-bottom water remains oxic.

The decomposition of settled organic carbon is the key factor controlling the redox-sensitive sediment processes, i.e. the coupled nitrification-denitrifiction process and the binding of phosphorus (P) with ferric iron oxides Fe(III). Nitrification and denitrifiction occur only under aerobic conditions; nitrogen is thereby leaving the system in gas form as N_2. The efflux of nitrogen (N) to the water begins when oxygen is depleted due to CO_2 formation.

In the absence of oxygen, Fe(III)-oxides are reduced through microbial mechanisms to ferrous iron (Fe(II)), which is unable to bind phosphorus. The iron-trapped P in the sediment is subsequently released to the water. This is the so called P-internal loading. The mineralization of organic matter provides the main energy source for these microbial activities. Therefore, there is a direct link between the mineralization of organic carbon and the sediment nutrient cycling.

Phytoplankton detritus settling from the surface is modelled by three detritus variables C_{det}, N_{det} and P_{det} (Fig.13). It becomes volatile sediment when it reaches the bottom and is accounted for in three other variables C_V, N_V and P_V. Iron-bound P is accumulated in another variable, P_{FeV} (Fig.13). The equivalence between species in Kiirikki *et al.* (2006) and Neumann & Schernewski (2008) is summed up in Table 3.

Here also, three numerical formulations are tested for the internal loading. Their full expressions are given in the coming detailed description. Formulation (4) directly corresponds to Kiirikki *et al.* (2006)'s hypothesis. Formulation (5) is an adjustment to Neumann & Schernewski (2008)'s hypothesis. And formulation (6) is consistent with (3).

Detailed description

The settling velocity of detritus nutrients, s, is assumed constant and equal to $1.0\ m/day$ (Heiskanen & Tallberg, 1999). The same value is used for sedimentation, i.e., settlement that reaches the sea floor.

The mineralization of detritus is a temperature-dependent process which, here, releases dissolved inorganic nitrogen (DIN) (including ammonium (NH_4) and nitrate (NO_3)) and dissolved inorganic phosphorus (DIP) regardless of the aerobic/anaerobic conditions (Kristensen *et al.*, 1995). The mineralization rates for the water-borne detritus, β and γ are the same as those presented in section 2.4.1. The mineralization rate for the sediment detritus is given as:

$$\mu = \mu_{max}.f_{T\mu}(T)$$

where the maximum mineralization rate is $\mu_{max} = 0.04\ d^{-1}$ (Pett, 1989) and $f_{T\mu}$ is defined like $f_{T\beta}$ and $f_{T\gamma}$.

The *critical point of CO_2-flux* (C_{Cr}) is the threshold between aerobic and anaerobic conditions. If the mineralized carbon in the sediment $\mu.C_V$ exceeds C_{Cr}, all the sediment processes become anaerobic. This parameter is obtained from the experimental measurements and calculations by Kiirikki *et al.* (2001). The proposed range spans from 200 to 470 $mgC/m^2/day$. $200 - 250\ mgC/m^2/day$ is recommended for shallow water bodies as the GoF.

A fraction fr_{dn} of the mineralized nitrous sediment flux is denitrified and exits the system as N_2. A fraction fr_P of the mineralized phosphorous sediment flux is chemically bound to Fe(III) and accumulated in the P_{FeV} variable. These two parameters are here numerically estimated to 70% by Kiirikki *et al.* (2006), which yields:

$$fr_{dn} = fr_P = \begin{cases} 0.7 \text{ when } \mu.C_V < C_{Cr} \\ 0. \text{ when } \mu.C_V > C_{Cr} \end{cases}$$

A last parameter, γ_{pin}, fixes the ratio between the mineralized P from P_V and the internal loading from P-Fe. It is obtained by Kiirikki *et al.* (2006) as:

$$\gamma_{pin} = \begin{cases} 0. \text{ when } \mu.C_V < C_{Cr} \\ 3.75 \text{ when } \mu.C_V > C_{Cr} \end{cases}$$

The corresponding internal loading is:

$$\frac{\gamma_{pin}}{h_2}\mu(t).P_V \tag{4}$$

To assess the internal loading simulation performance of the sediment module in comparison with the formulation from Neumann & Schernewski (2008), two other hypothesis are tested in addition to the previous formulation given. A finite P storage is considered for the internal loading as it is proposed by Neumann & Schernewski (2008):

$$\frac{\gamma_{pin}}{h_2}.\mu(t).P_{FeV} \tag{5}$$

Table 5: Table of sources for initial values.

Variable	Source
c_C	Kiirikki *et al.* (2001)
c_A	Kiirikki *et al.* (2001)
DIN	monitoring data (extrapolated)
DIP	monitoring data
A_m	monitoring data
Ni_m	monitoring data (extrapolated)
C_{det}	trial
N_{det}	trial
P_{det}	trial
D	trial
C_V	Virtasalo & Kotilainen (2008) and trial
N_V	Virtasalo & Kotilainen (2008) and trial
P_V	Virtasalo & Kotilainen (2008) and trial
P_{FeV}	Virtasalo & Kotilainen (2008) and trial
S	Virtasalo & Kotilainen (2008) and trial
I_P	Virtasalo & Kotilainen (2008) and trial
O_2	monitoring data

As for the last alternative an infinite source of P but with a constant release rate is formulated as below:

$$\frac{\gamma_{pin}}{h_2}\mu(t).P_{FeV0} \tag{6}$$

The burial rate for C_V and N_V is $0.0001\ d^{-1}$ (Pett, 1989). No burial is considered for P_V to preserve the infinite source of P in the sediment.

The corresponding rates are expressed against their equivalent in the other competing model in Table 4.

2.6 Implementation

2.6.1 *Driving forces*

Two main drivers are needed to evaluate the parameters in the equations: temperature and solar radiation.

Temperature has been collected from data records in the Finnish monitoring stations Haasapaari and Längden (Fig.3). Averages of the temperature above and below 20 m are used as temperatures for the surface and deep water. The stations are granted different roles based on their respective locations: Haapasaari is used for temperature driving and validation of the predictions, Längden is used to get realistic boundary conditions with the open sea.

An estimation of the ice cover periods is obtained from the temperature series in the surface box. A threshold is adjusted to approximately fit the annual ice cover duration given by Schiewer (2008).

Solar radiation are estimated by the averaged quantities proposed on the European Commission's Joint Research Center's website: PVGIS (2011). The average radiation profile for one year is repeated periodically every year of the simulation.

2.6.2 *External nutrient loads and boundary conditions*

The external nutrient loads are estimated according to the annual values given in Schiewer (2008). The annual input is spread to be injected continuously along with the freshwater inflow.

The records at the monitoring station Längden (Fig.3) are interpolated to obtain continuous boundary conditions with the Baltic Proper. DIP is directly in the record as phosphate concentration measurements. DIN is not explicitly recorded, but is estimated as being a constant fraction r_N of the total nitrogen time series. Ammonium quantities are given and the nitrate is taken as the difference between DIN and ammonium. Chlorophyll-a is recorded and gives a way to estimate the amount of algae (Kuusisto *et al.*, 1998). Oxygen is also present in the time series. Non-recorded variables, i.e., detritus variables, are assumed to be zero by default.

The atmospheric deposition of nitrogen is negligible in front of the external load (HELCOM, 2004).

Similarly to Neumann *et al.* (2002), the oxygen dissolution at the surface is expressed as a flux targeting saturation conditions:

$$\dot{O}_{2\ atm\ dissol} = p_{vel}(O_{sat} - O_2)$$

where $O_{sat} = \frac{a_0}{O_{norm}}(a_1 + a_2.T)$.

2.6.3 *Initial values*

The initial values are evaluated, by order of preference, from the records at the Haapasaari monitoring station, from literature values or by trial and error. The sources for each variable are described in Table 5.

2.6.4 *Equation solver and data processing*

Solving the ODEs has been performed with the embedded numerical solver in the computational software *Mathematica*.

The analysis of the hydrodynamic simulation to obtain the flow aggregates and the processing of the data records have been achieved via scripts in *Python*, especially with the computational libraries, *Numpy*, *Scipy* and the graphical library *Matplotlib*.

2.6.5 *Parameter estimation*

The model's internal parameters are tested to obtain the best fit and assess the robustness of the model. This calibration phase is carried on year 2004 alone. The parameters with the most uncertainty are identified as the oxygen threshold O_{2T}, the ratio $r_N = \frac{DIN}{\text{tot}-\text{N}}$ and the internal loading rate l_{i0} for the formulations based on Neumann & Schernewski (2008), and as the oxic/anoxic threshold value for the mineralization of carbon C_{Cr}, r_N and the internal loading rate γ_{Pin} for the formulations based on Kiirikki *et al.* (2006). Each of them is assigned a possible range of values that is automatically scanned to obtain the best fit and evaluate the sensitivity for each formulation. Other variables that might influence the simulations are also tested like fr_{dn} and fr_P.

After calibration on year 2004, a simulation is run for years 2000 to 2007 for validation. A point of interest is the stability of the model, i.e., its ability to dampen errors or to propagate them. These results are presented and discussed in the upcoming sections.

3 RESULTS AND DISCUSSION

3.1 Effect of the hydrodynamics

A prerequisite to any successful simulation is to rely on faithful hydrodynamics. One can see that the abuse of time averaging potentially hinders the stability of the simulation (Fig.14). A flow description averaged over the whole year does not grasp the mixing processes and produces an artificial accumulation of DIP in the bottom water (Fig.14). A flow function averaged monthly does not render the occurrence of short duration mixing events and can hence fail to launch a cyclical ecosystem (Fig.14). The first conclusion is thus that a successful biogeochemical water quality simulation is conditioned by an underlying daily flow description (Fig.14).

3.2 Review of six model formulations

The results obtained for the 6 formulations (Table 1) after calibration are presented in Fig.15, 16, 17, 18, 19 and 20 against the available time series at the monitoring station Haapasaari for the Algal concentration (top left), DIN (middle) and DIP (bottom). The oxic/anoxic switch for the sediment processes are also displayed (top right) along with the corresponding threshold value (dotted lines).

Averages of sediment fluxes, primary production and C/N ratios are given in Table 6 and 7 against literature values collected in Schiewer (2008).

3.2.1 *Formulation (1)*

Oxygen prediction shows overshoots and delays but produces stable inter annual transitions (Fig.15).

The winter accumulation of DIN at the surface is in accordance with the values given by Schiewer (2008): $98 - 280\ mg/m^3$. There is no long term DIN depletion at the surface in summer (Fig.15). The model underestimates ammonium release and denitrification (Table 6) as well as the bottom water DIN, which is expected to oscillate between $100 - 170\ mg/m^3$ (Kiirikki *et al.*, 2001). DIP and the sediment phosphate release, on the contrary, are globally underestimated (Fig.15 and Table 6).

As a consequence, the ecosystem growth is P-limited instead of N, which explains that the primary production and the biomass are globally underestimated (Table 7 and Fig.15). The spring blooms of algae are captured —although underestimated— whereas the summer blooms of cyanobacteria are not (Fig.15).

3.2.2 *Formulation (2)*

Oxygen prediction shows no significant difference with formulation (1).

The winter value of DIN at the surface is correctly in the given range (Fig.16 and 17). Sediment ammonium release is overestimated but depletion of DIN at the surface still happens in the summer (Table 6, Fig.16 and 17). DIP is present in excess in the winter time at the surface. It however does not accumulate and reaches back low concentrations for every year

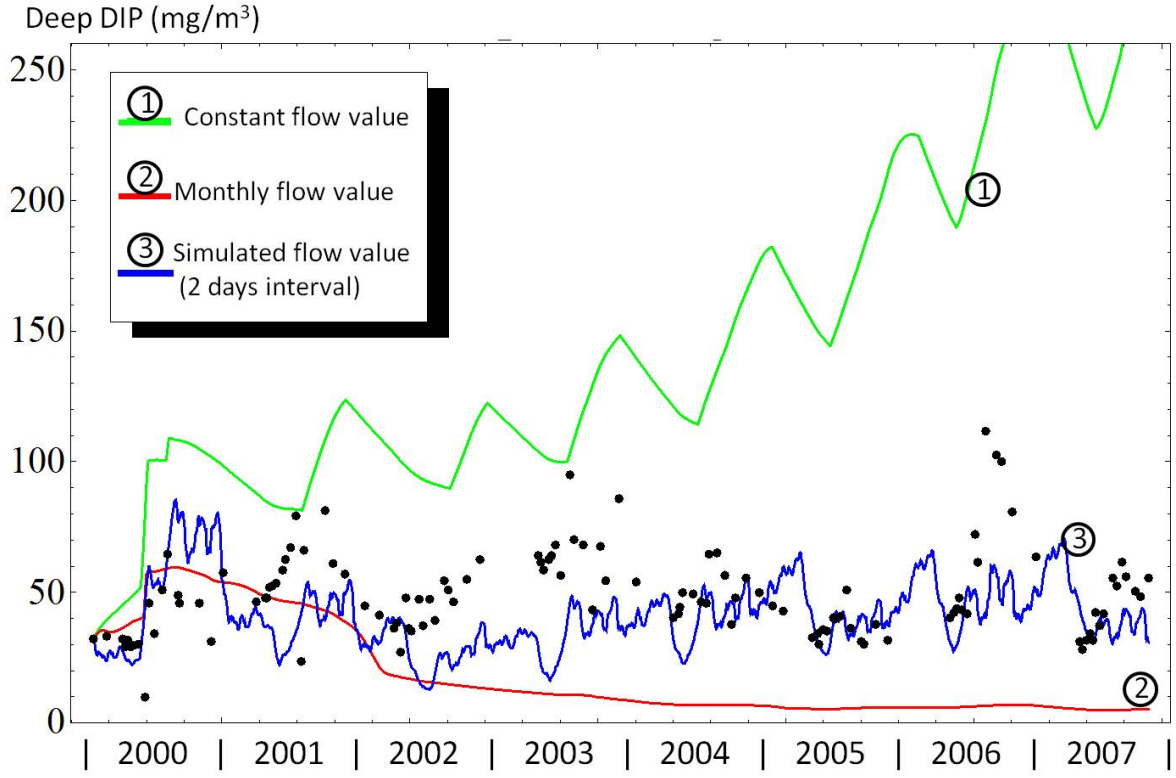

Fig. 14: Deep DIP for 8 years of simulation (2000-2007) under different flow conditions (the biogeochemical transformations are all according to formulation (4), i.e. to Kiirikki et al. *(2006)), against the measurements at the monitoring station Haapasaari (background dots).*

Table 6: Table of average sediments characteristics in the GoF, in literature and from the simulations according to the six internal loading formulations described in section 2.5).

Sediment characteristic	unit	Schiewer (2008)	(1)	(2)	(3)	(4)	(5)	(6)
C_V/N_V	(weight ratio)	10.5	-	-	-	7.4	7.4	7.4
Phosphate release	$mg\ P/m^2/day$	5.5	2.0	4.3	4.5	4.8	1.6	1.7
Ammonium (or DIN) release	$mg\ N/m^2/day$	23	15.5	33	34	34	12.5	13.9
Denitrification	$mg\ N/m^2/day$	6.3	0.5	0.9	0.9	5.9	9.9	10.3

Table 7: Table of average water characteristics in the GoF, in literature and from the simulations according to the six internal loading formulations described in section 2.5).

Water characteristic	unit	Schiewer (2008)	(1)	(2)	(3)	(4)	(5)	(6)
C_{det}/N_{det} surface	(weight ratio)	4.2 - 6.9	-	-	-	7.5	7.6	7.6
C_{det}/N_{det} deep	(weight ratio)	4.2 - 6.9	-	-	-	8.0	8.0	8.0
Primary production	$g\ C/m^2/year$	75 - 110	42	102	108	134	76	79

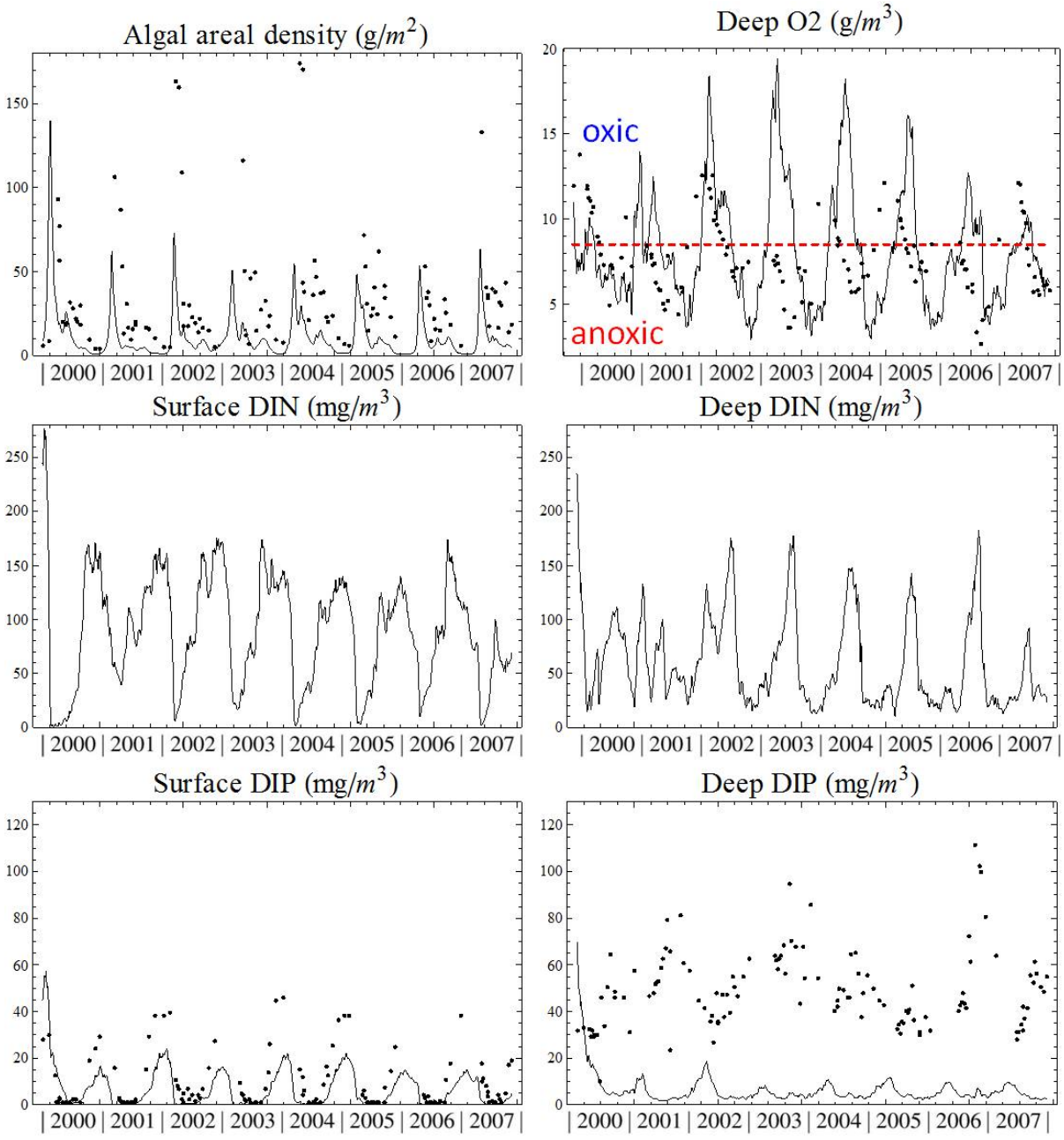

Fig. 15: Results for 8 years of simulation (2000-2007) according to internal loading formulation (1), against the measurements at the monitoring station Haapasaari.

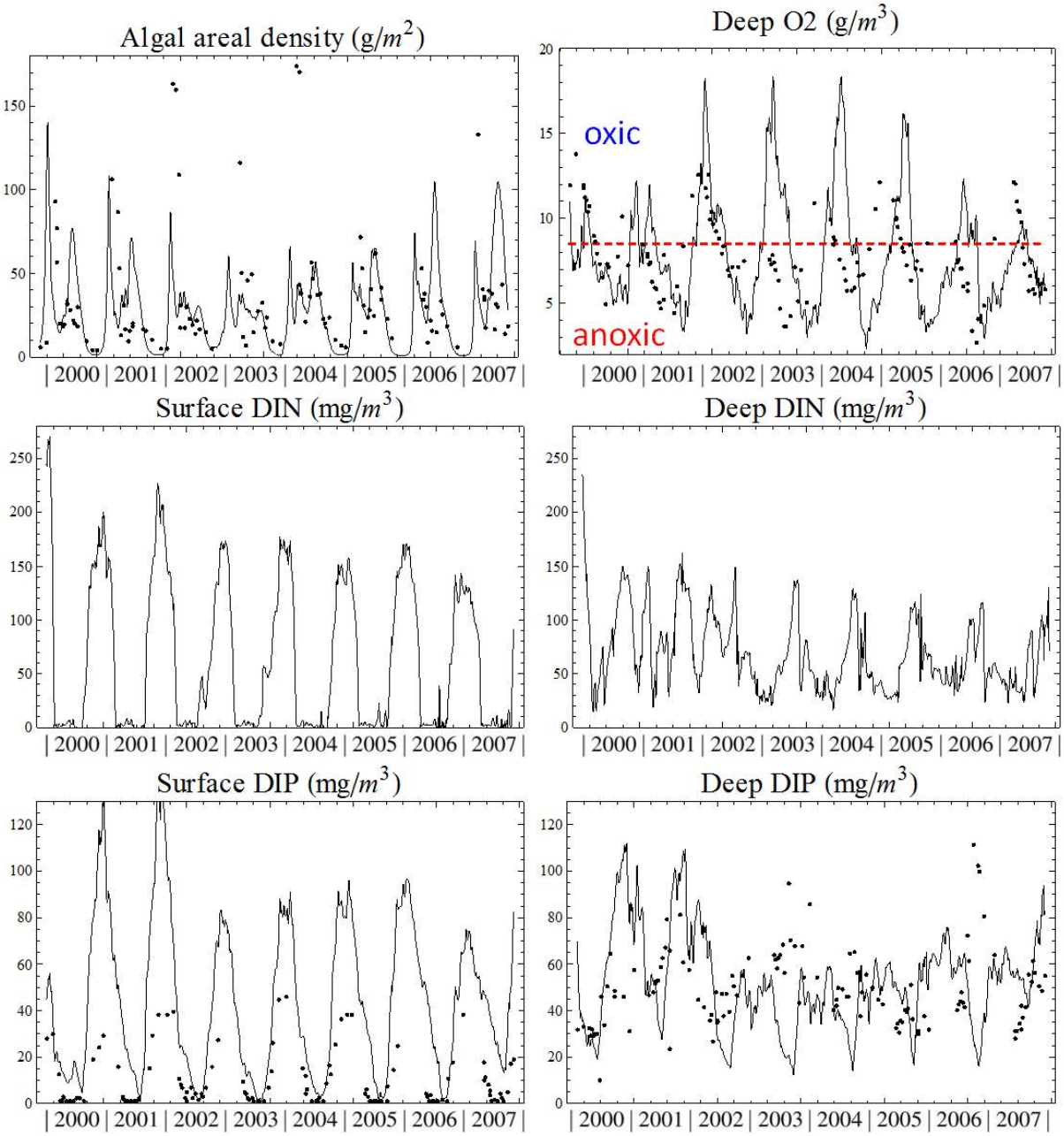

Fig. 16: Results for 8 years of simulation (2000-2007) according to internal loading formulation (2), against the measurements at the monitoring station Haapasaari.

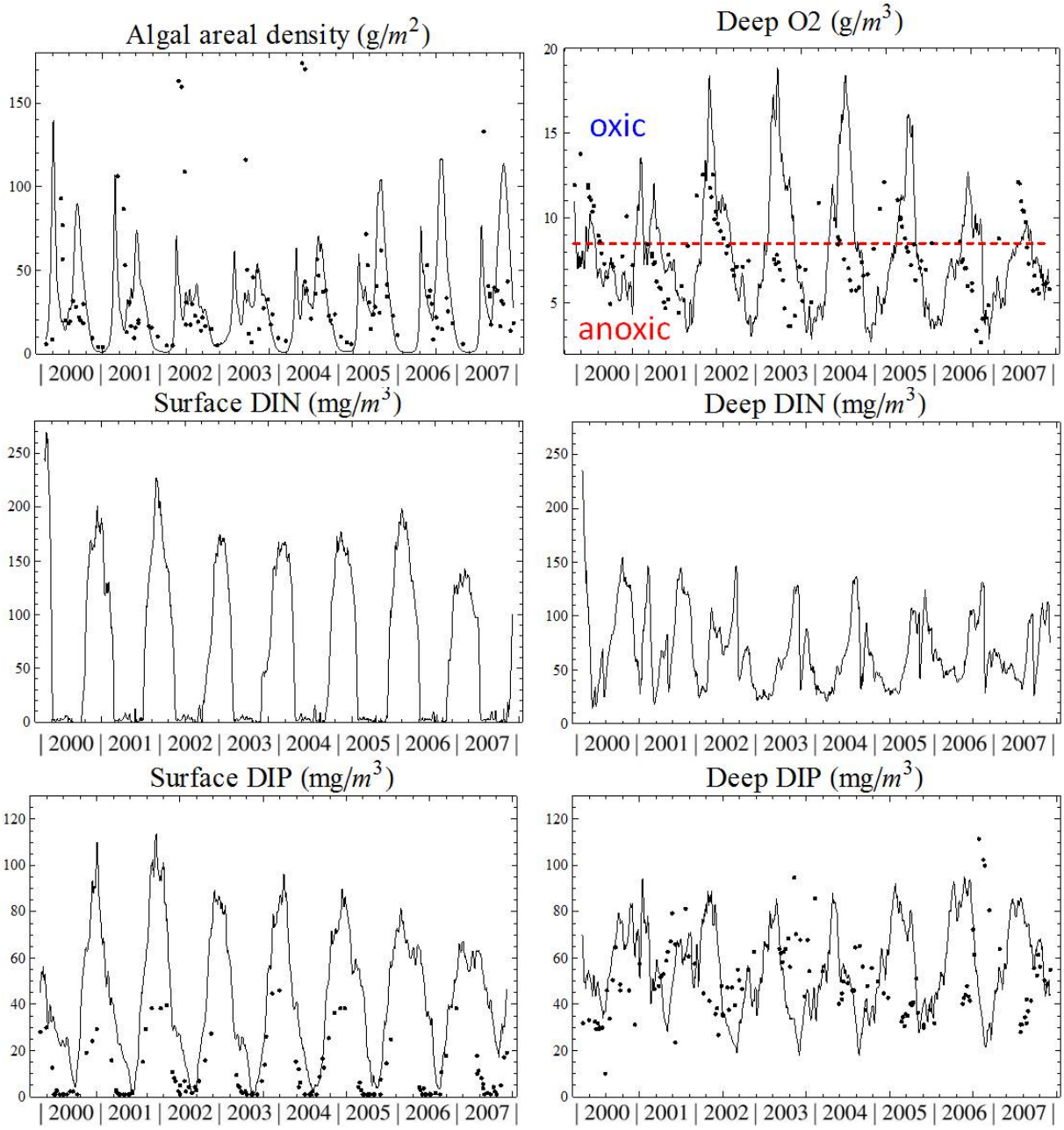

Fig. 17: Results for 8 years of simulation (2000-2007) according to internal loading formulation (3), against the measurements at the monitoring station Haapasaari.

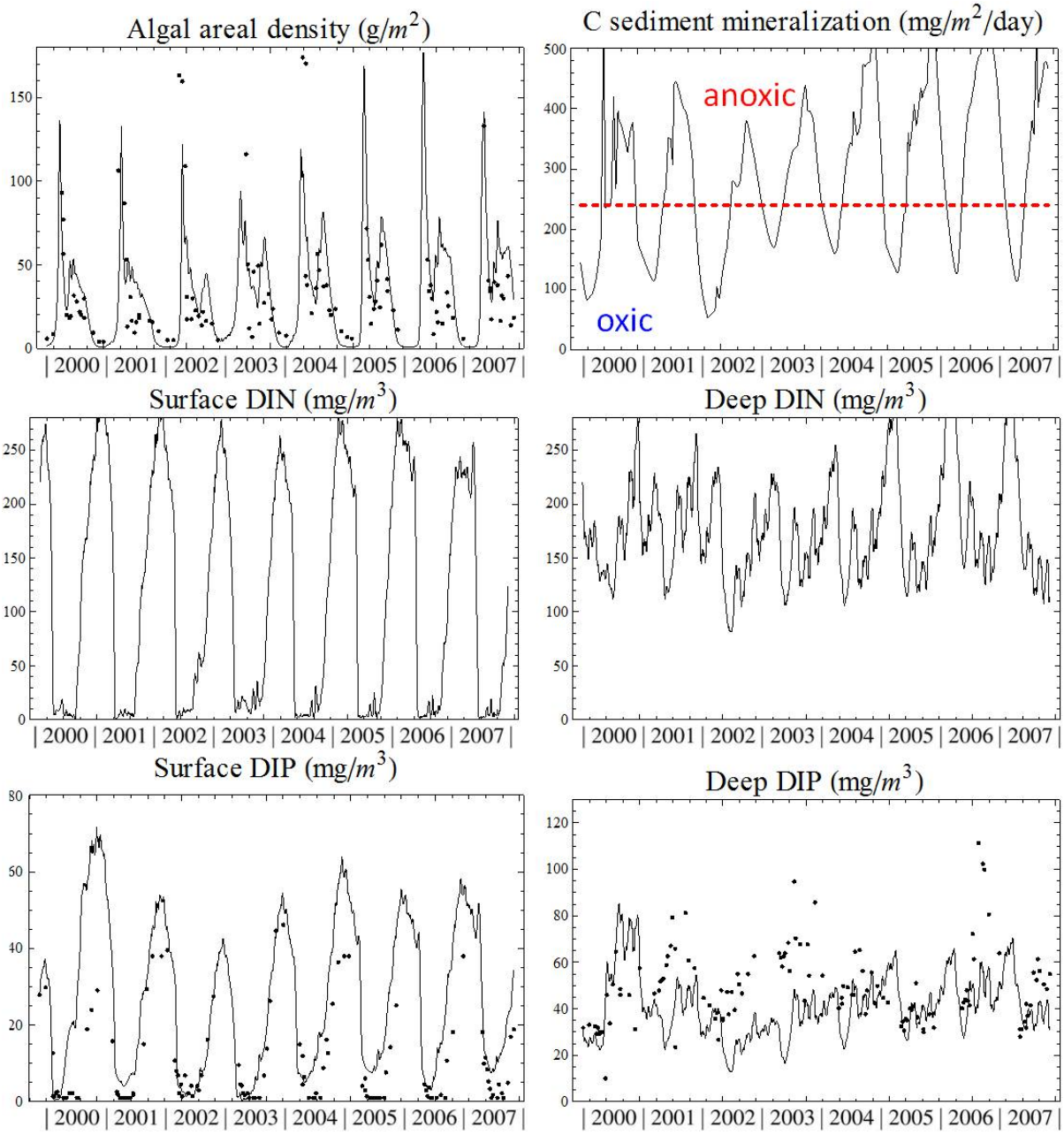

Fig. 18: Results for 8 years of simulation (2000-2007) according to internal loading formulation (4), against the measurements at the monitoring station Haapasaari.

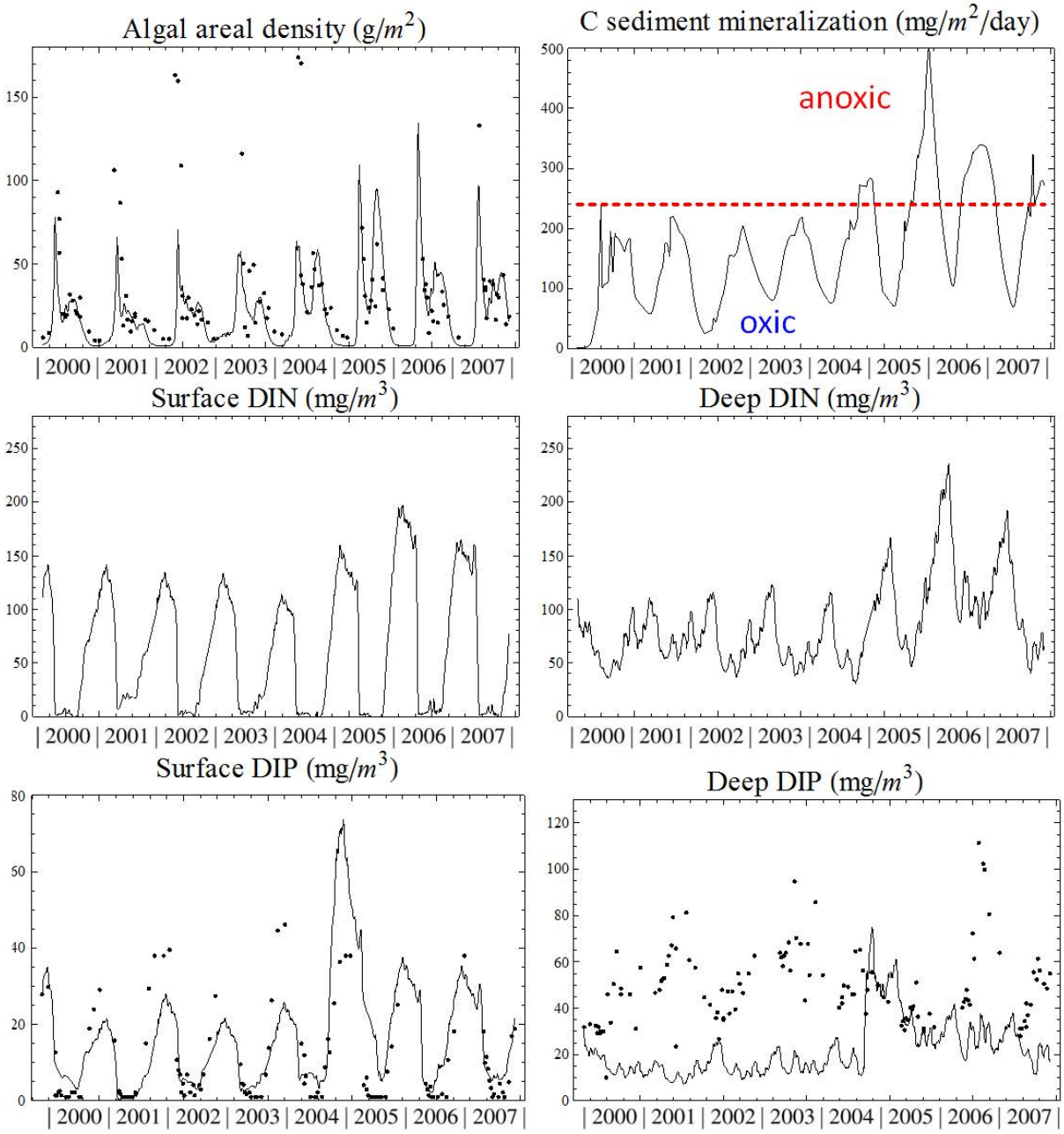

Fig. 19: Results for 8 years of simulation (2000-2007) according to internal loading formulation (5), against the measurements at the monitoring station Haapasaari.

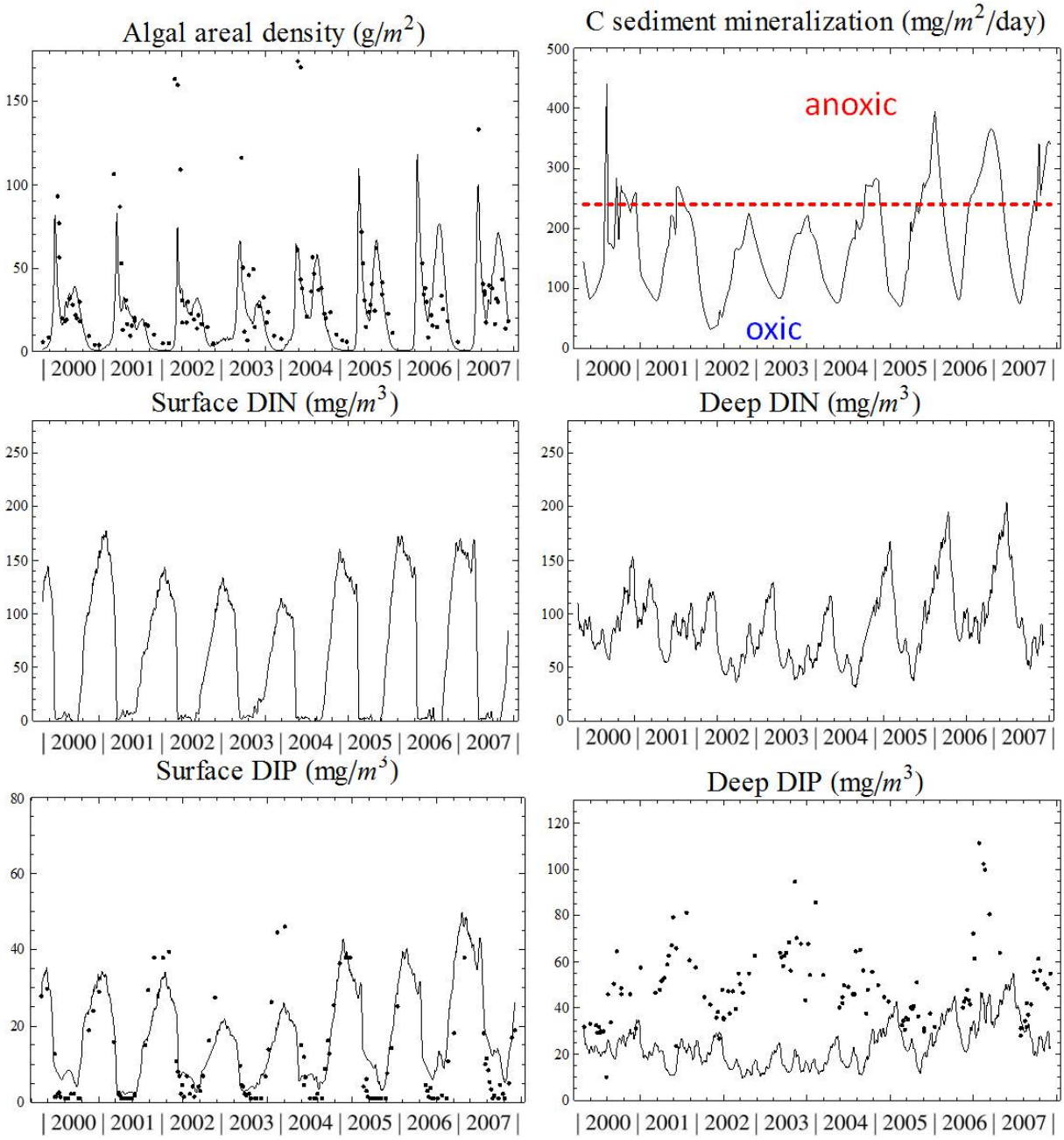

Fig. 20: Results for 8 years of simulation (2000-2007) according to internal loading formulation (6), against the measurements at the monitoring station Haapasaari.

but the last one (Fig.16 and 17). The values obtained for DIP in the deep water and the average phosphate release rate show that the internal loading is rendered (Table 6, Fig.16 and 17).
These observations diagnose a N-limited ecosystem, which stands with the published literature (Schiewer, 2008). The biomass prediction ends in the observed range (Table 7). Both spring and summer algal blooms are captured even though the spring bloom is clearly underestimated (Fig.16 and 17).

3.2.3 *Formulation (3)*

Observations are in almost every aspect similar with those under formulation (2).
The only difference is in the deep DIP, which is less subject to high accumulations in the years 2000 and 2001.

3.2.4 *Formulation (4)*

The simulated algal areal density of biomass is highly consistent with the measured data in the eastern Gof. Generally spring bloom peaks follow the measurements. However, they are slightly underestimated from 2002 to 2004. The low peak values are directly linked to the diminished DIN concentrations in the model during the same period. The summer bloom peaks are well aligned with the measurements. They are slightly elevated in 2002 to 2004 due to the overestimation of DIP concentrations. DIP concentration controls the summer blooms which are mainly N-fixers cyanobacteria. Surface DIN values are close to zero for most springtime implying the fact that the other algae take up the entire DIN available. The model shows a reasonable capability of maintaining deep DIN values in the acceptable range.
C sediment mineralization shows the daily efflux of mineralized carbon leaving the sediment in comparison with critical point of carbon (the dashed line represents C_{Cr}). As a direct consequence of nine-month anoxic periods ($\mu.C_V > C_{Cr}$) during years of 2004 to 2007, large algal biomass peak values are observed. Surface DIP values are highly compatible with the measured data. They are relatively close to zero in summertime due to cyanobacteria consumption. In 2002, the calculated DIP concentration sharply increases right after experiencing the first jump to anaerobic condition in springtime. Simulated deep DIP concentration clearly follows the episodic trend of C sediment mineralization efflux. The model simulates DIP values with an up to standard accuracy.

3.2.5 *Formulation (5)*

In general, the primary production is low. Spring bloom peak values are a long way to reality. However, the model reproduces summer bloom levels efficiently. The biomass production is N-limited (Fig.19). Four anoxic episodes merely happen during the last four years of simulation. Surface DIN values are underestimated during wintertime. DIN in the surface is depleted ($< 5\ mg\ m^{-3}$) in the springtime of the entire simulation period (Fig.19). The average simulated DIN release from the sediment ($12.5\ mg\ N/m^2/day$) is lower than the flux value ($23\ mg\ N/m^2/day$) suggested by Schiewer (2008) (Table 6). DIP concentrations in the surface and deep water are both underestimated in the first four years of simulation. An overestimation of DIP peak value happens in accordance to the occurrence of the first anoxic event in the year 2004. Even though the model maintains surface DIP in 2005-2007, will not likely sustain following the decreasing trend of DIP in the surface and deep water as well (Fig.19). The lowest average phosphate release ($1.6\ mg\ P/m^2/day$) is obtained in this formulation with a finite source of P (bound to iron) in sediments (Table 6).

3.2.6 *Formulation (6)*

The model performance is more compatible with formulation (4). However, underestimations of DIN both in the surface and deep water cause low biomass production during springtime. In comparison to the formulation (5) more anaerobic episodes are observed but with shorter durations. DIP values in the surface water are lower than the measured data during oxic conditions, whereas, phosphate concentrations released from sediments are always underestimated. The ecosystem model is limited by N (Fig.20).

3.3 Comparison of internal loading flux expressions

3.3.1 *Formalism and formulation (1) (or (5) respectively)*

One can judge the impact of the flux expression by comparing the results of formulations (1),

(2) and (3) together (or (4), (5) and (6) respectively). Let's introduce a common formalism for the iron sediments to look at the internal loading. Let I_P be phosphorus bound to iron in the sediments. The mass balance for I_P yields:

$$\frac{\mathrm{d}I_P}{\mathrm{d}t} = f^+_{eco} + f^+_{other} - f^-_{burial} - f^-_{int}$$

where f^+_{eco} is phosphorus from the ecosystem's losses trapped by iron, f^+_{other} is phosphorus form other sources bounding to iron, f^-_{burial} is the amount of iron phosphorus reaching deep stable sediments and f^-_{int} is the contribution to internal loading released to the water. Formulation (1) (or (5) respectively) consists in supposing $f^+_{other} = 0$ and $f^-_{int} = k_{int}(Ox).I_P$ where $k_{int}(Ox)$ depends only on the oxic status Ox and not on I_P. In other terms, there is no other source of phosphorus than the fresh detritus produced by the surface ecosystem and the internal loading is assumed to follow a linear first order release when conditions become anoxic.

Fig.21 shows that under formulation (1), I_P rapidly reaches values close to 0 and Fig.15 points that the levels of DIP are underestimated, especially in the bottom water. Scenario (5) shows the same behavior apart from the massive anoxic release during year 2004 that is diffused in 2 years. These observations indicate that a source of phosphorus is missing to sustain the system in the ranges displayed by the data. Another assumption must be made for f^+_{other}.

3.3.2 *Limit case: formulation (3) (or (6) respectively)*

In a second attempt, this study explores the case where f^+_{other} is tailored to sustain $\frac{\mathrm{d}I_P}{\mathrm{d}t} = 0$, i.e. $I_P = I_{P0}$. One can point that to sustain such a condition, the other source of phosphorus is never bounded and can potentially become very large. The internal loading is still estimated by $f^-_{int} = k_{int}(Ox).I_{P0}$ which corresponds to formulation (3) (or (6) respectively). I_P is constant here by definition (Fig.21). Fig.17 shows that the range of simulated deep DIP is lifted to a more realistic range of values. However, one may argue that a source releasing phosphorus with a constant source concentration yields brusque variations in the deep water DIP concentration that cannot be observed in the measured series (Fig.17). Improvements can be made to achieve a more seasonal and less abrupt source of phosphorus.

3.3.3 *New hypothesis: formulation (2) (or (4) respectively)*

Kiirikki *et al.* (2006) proposes such a modification by correlating the internal loading to the amount of fresh detritus in the sediments $s_R.S$ in the Neumann et al. formalism (P_V in Kiirikki et al's formalism) instead of the iron-bound phosphorus itself. The source term f^+_{other} needs not explicitly be expressed but is assumed to provide sufficiently to sustain the internal loading as (formulation (2)):

$$f^-_{int} = \gamma_{Pin}.L_{SA}.s_R.S$$

(or as $f^-_{int} = \gamma_{Pin}.\mu.P_V$ for formulation (4)). Simulation (2) reaches a similar level to the previous formulation (3) with a constant source for the deep DIP levels (Fig.16 and 17), whereas formulation (4) shows some improvements from formulation (6) (Fig.18 and 20).

The progress made by shifting from formulation (1) to (2) can be observed in the same frame in Fig.22, 23, 24 25 and 26. One can read that the absence of the unknown source under (1) has the ecosystem running with too low nutrient concentrations and too scarce algal populations with no opportunity to lift itself to the right range.

It is of interest to underline under (2) (or (4) respectively) like in the previous limit case (3), the other source of phosphorus f^+_{other} is potentially infinite and the variable I_P is used here only to keep track of the amount of phosphorus that has been permanently provided by this unknown source (Fig.21).

3.4 Comparison of model structures: O_2/implicit vs. C/explicit

3.4.1 *General comparison*

After reviewing all formulations, (2) and (3) show the best performance for the models based on the oxygen concentration and (4) has the edge for the carbon-based models. (2) and (4) are consistent in their numerical definition of the internal loading flux. They are hence evaluated comparatively in Fig.22, 23, 24, 25 and 26 to the available data in order to assess the impact of the model structure for a similar internal loading flux expression.

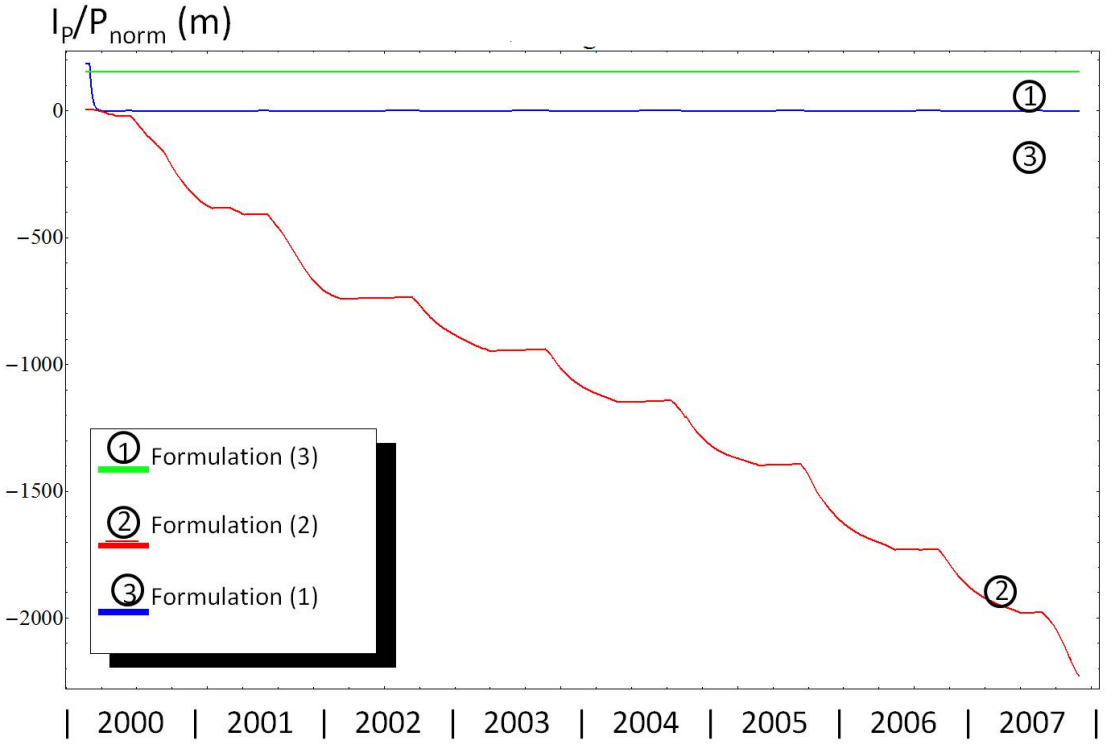

Fig. 21: Amount of iron-bound phosphorus in the sediments under formulations (1), (2) and (3), normalized by concentration P_{norm}.

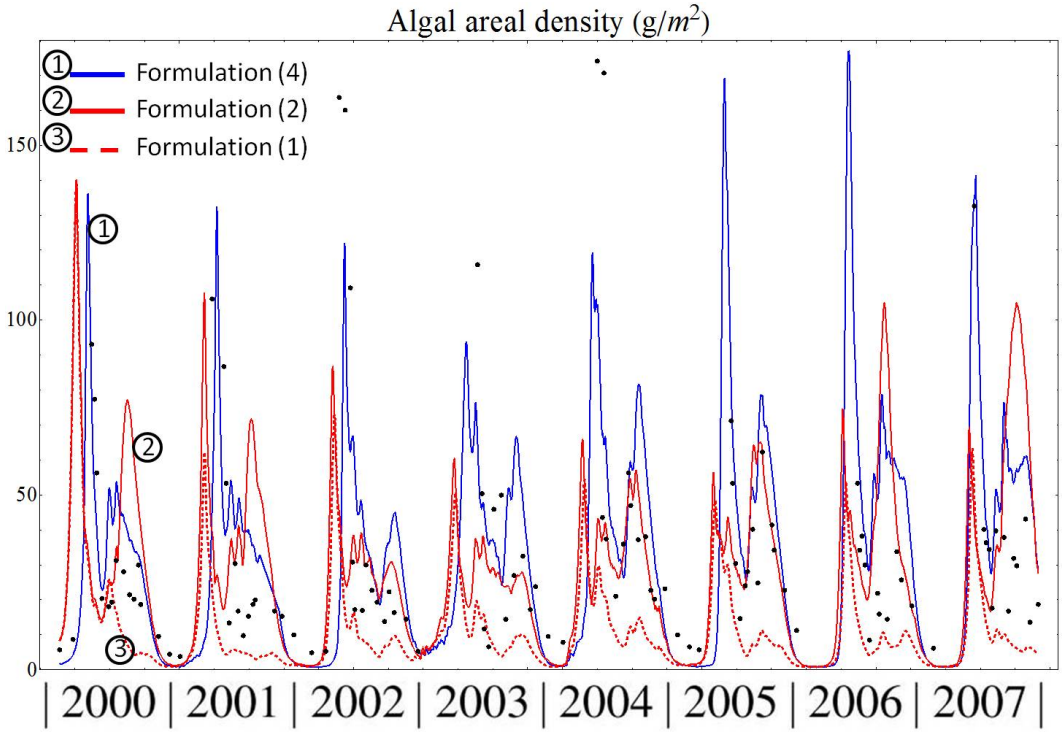

Fig. 22: Modelled algae for the years 2000-2007 according to formulations (1), (2) and (4) (dashed red curve, continuous red curve and continuous blue curve respectively).

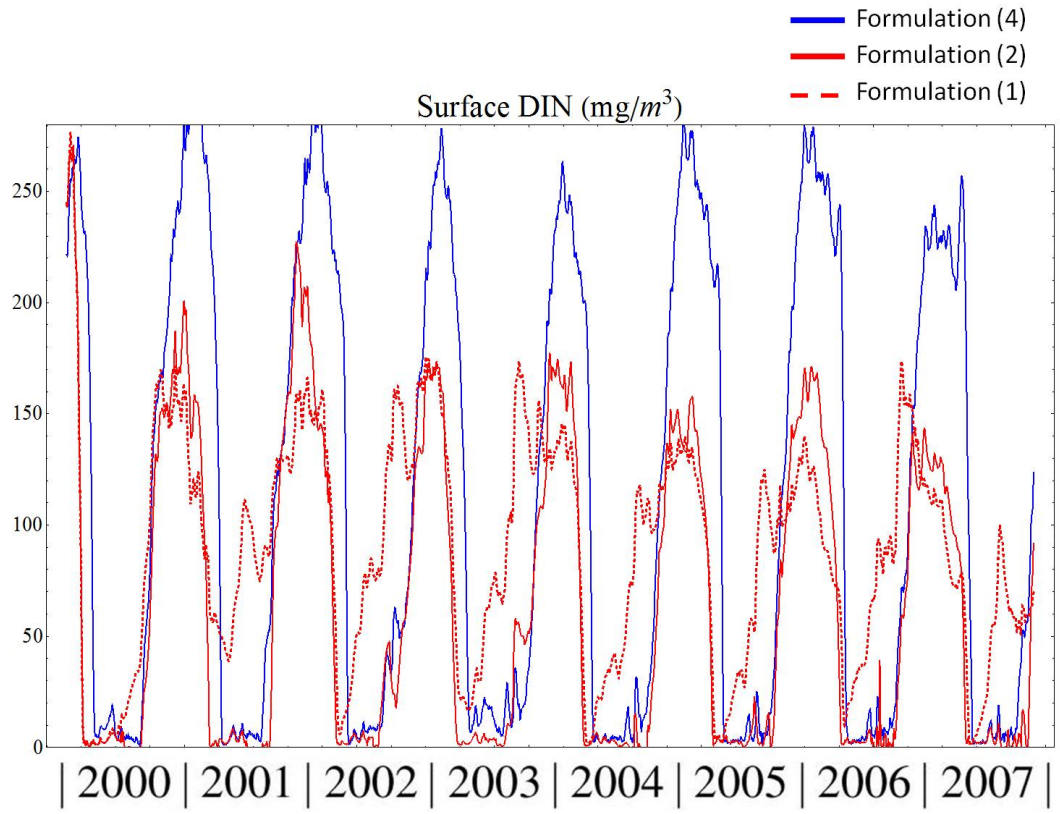

Fig. 23: Modelled surface DIN for the years 2000-2007 according to formulations (1), (2) and (4) (dashed red curve, continuous red curve and continuous blue curve respectively).

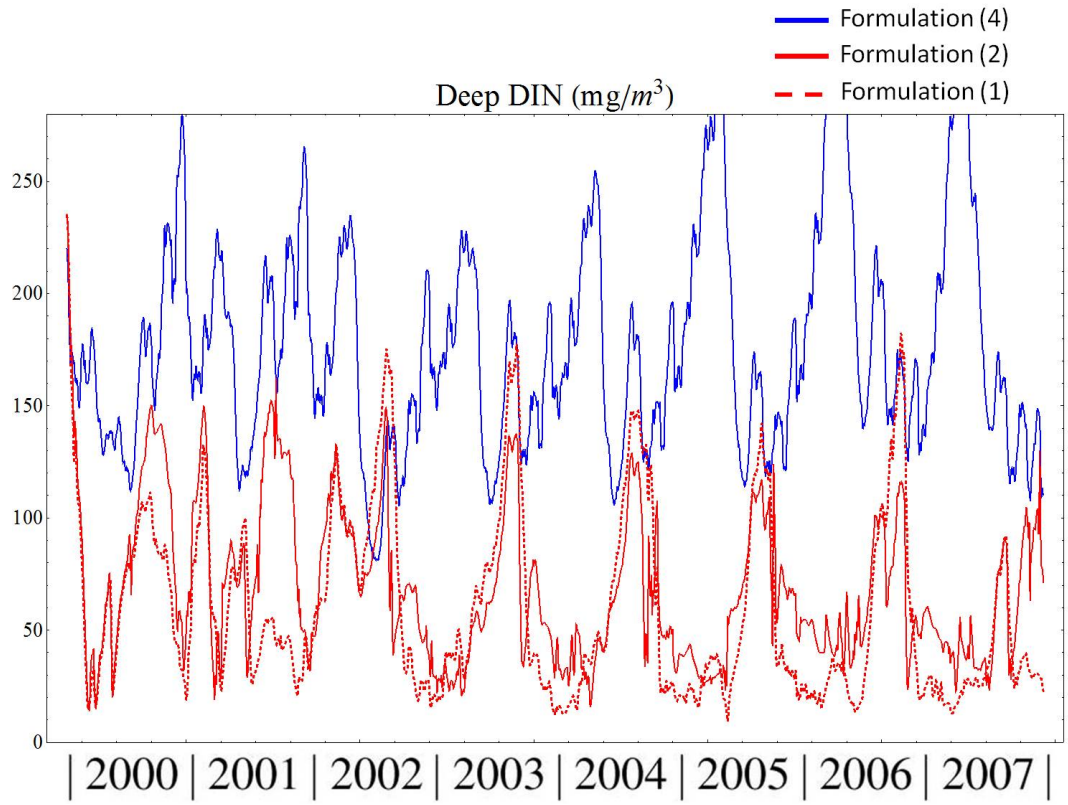

Fig. 24: Modelled deep DIN for the years 2000-2007 according to formulations (1), (2) and (4) (dashed red curve, continuous red curve and continuous blue curve respectively).

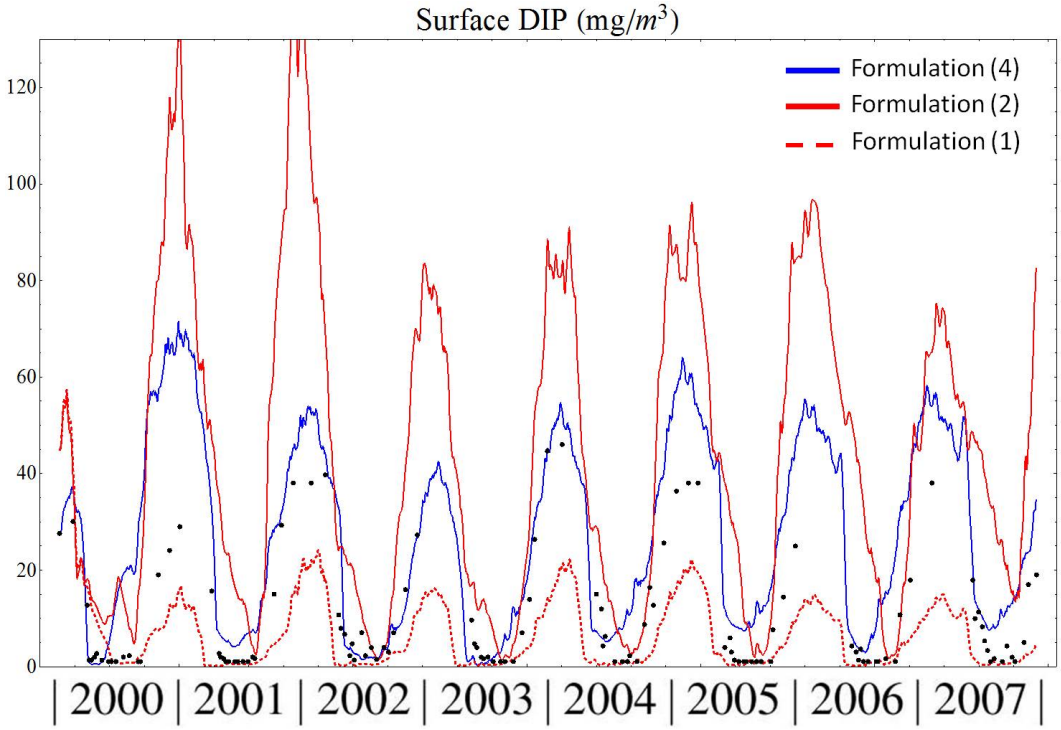

Fig. 25: Modelled surface DIP for the years 2000-2007 according to formulations (1), (2) and (4) (dashed red curve, continuous red curve and continuous blue curve respectively).

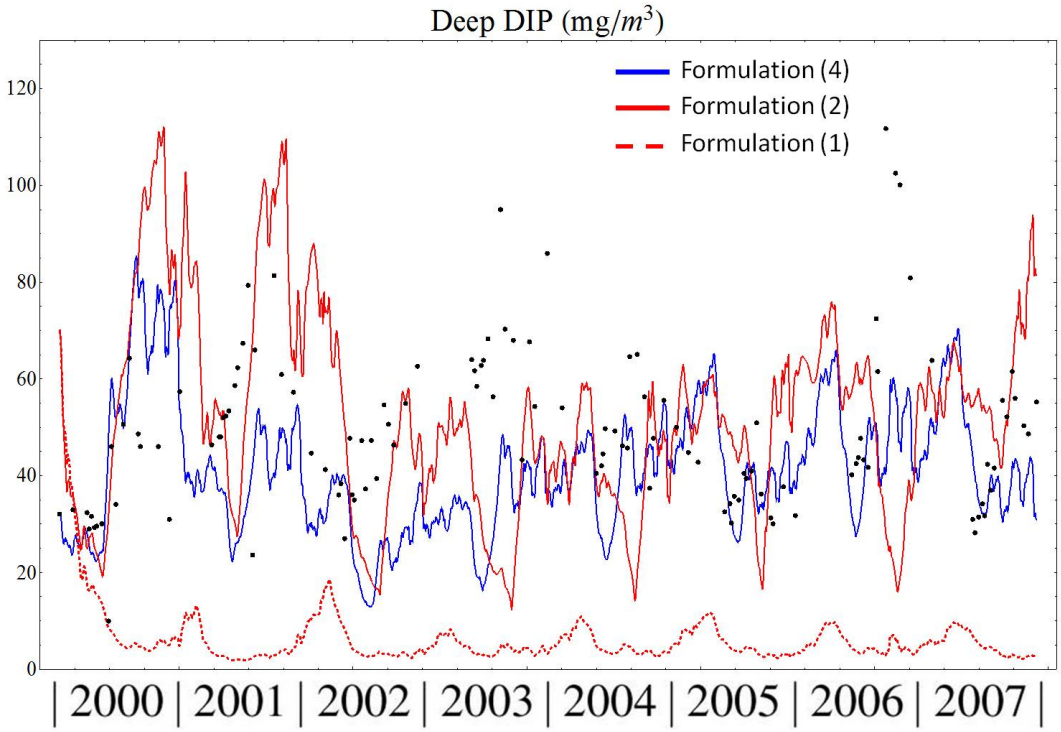

Fig. 26: Modelled deep DIP for the years 2000-2007 according to formulations (1), (2) and (4) (dashed red curve, continuous red curve and continuous blue curve respectively).

Concerning the algal density, (4) has a better forecast of the spring blooms and both formulations are comparable for the summer blooms (22). However, primary production following (2) falls in the accepted range when (4) gives a slight overestimation (7). The formulation based on a carbon switch has thus an advantage to grasp the dynamic effects when the oxygen-based formulation gives a better long-term average.

Both surface DIN concentrations fall into the acceptable range (Fig.23). However, the winter value according to (2) recedes gradually every year, which provokes excessive summer algal blooms in the last two years of the simulation (Fig.23 and 22). (4) shows a slight overestimation of the bottom DIN, when levels are clearly underestimated with hypothesis (2).

DIP at the surface is closely predicted by formulation (4) whereas (2) produces significant overshoots. The performance for deep water DIP are comparable.

3.4.2 *Sensitivity analysis*

The model performance to simulate DIP (or PO respectively) at the surface is studied by using the E_{NS} objective function (Seibert, 1997):

$$E_{NS} = 1 - \frac{\sum (DIP_{obs} - DIP_{sim})^2}{\sum (DIP_{obs} - \overline{DIP}_{obs})^2}$$

The value for a perfect fit is 1.

The sensitivity of the carbon-based model to its four internal parameters C_{cr}, fr_{dn}, fr_P and γ_{Pin} is investigated by running a Monte Carlo procedure for a thousand runs. As for C_{cr} a uniform distribution over $200 - 470\ mg\,C\,m^{-2}.d^{-1}$ is assumed as recommended by Kiirikki *et al.* (2006) for the Baltic Sea sediments. $E_{NS} \approx 0.5$ (Fig.27) shows that the model effectively simulates DIP concentrations but is still slightly biased. The deviation from presumed internal parameter $C_{cr} = 240\ mg\ C\ m^{-2}.d^{-1}$ for the GoF does not impair the model performance. The spatial variation of the critical point C_{cr} does not appear as a barrier to apply the carbon-based approach in other basins of the Baltic Sea. Sensitivity to fr_{dn} and fr_P is very limited as well, whereas γ_{Pin} requires some tuning.

The oxygen-based model has also been set for a Monte Carlo analysis with a thousand runs (O_{2T} is uniformly distributed over $7 - 12\ g.m^{-3}$). It shows a greater sensitivity to the critical threshold value O_{2T} (Fig.28). l_i displays a significant impact on the results as well.

3.5 Limitations of the study

3.5.1 *Limits of the model's geometry and structure*

The very simple geometrical structure grants advantages to flexibly test different biogeochemical formulations. However this simplicity comes with shortcomings. For example, the divide of surface and deep water as it is made (with the same area) implies that all the Gulf is treated as deep water. This very simplistic assumption is a strong limitation for a water formation that includes extensive shallow coastal areas. Moreover, the longitudinal gradients (west-east) of salinity and nutrients concentrations are neglected by the fully mixed boxes. The Gulf could be broken down to a greater number of boxes in the west-east direction for more accuracy. Finally, the mixing effect of anticlockwise horizontal circulation patterns reported inside the Gulf (Alenius *et al.*, 1998) is overestimated by the assumption of fully-mixed boxes.

3.5.2 *Limits of the comparison model/data*

Although coarsely grasping the environmental dynamics of the system, undertaking to model the GoF with two boxes introduces a significant level of abstraction. It is important to understand that the time series at the monitoring Haapasaari are locally accurate measurements. The comparison with abstract model averages should not be taken as a definite validation of the former. A validation in the strict sense would require the model to produce local predictions directly associable to the very station's location or the data to include statistics over a set of stations considered representative of the whole Gulf.

3.5.3 *Time resolution of the data*

Data from monitoring stations are available with a variable time frequency, usually once a month, sometimes more. Driving the boundary conditions and the temperature of the model with such data involves performing a linear interpolation of these measurements, which is necessary but introduces errors.

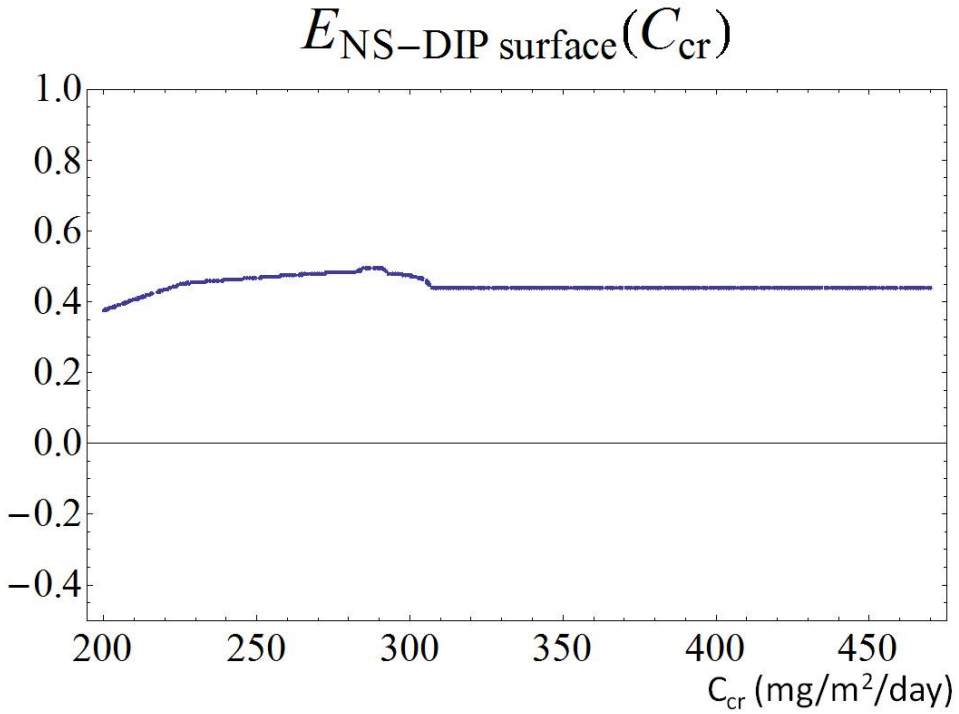

Fig. 27: Sensitivity of the model's surface DIP (formulation (4)) to the internal parameter C_{cr}.

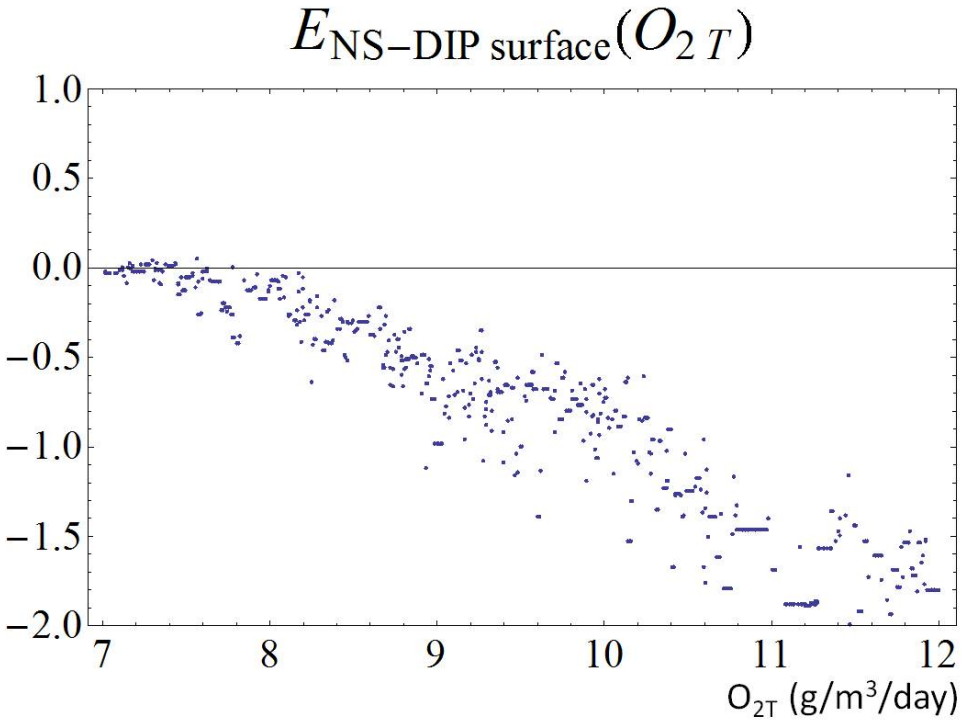

Fig. 28: Sensitivity of the model's surface DIP (formulation (2)) to the internal parameter O_{2T}.

3.5.4 Sediment transport

A strong implicit assumption, made in both biogeochemical cycle descriptions that are implemented here, is that the study area behaves like a deposition area. Assuming a net source of phosphorus in the sediments to maintain the phosphate release mitigates this simplification. Other processes are involved in the deposition of phosphorus in sediments like the erosion and redeposition of clay soils. One may argue that accumulation zones of phosphorus in the sediments are presumed to be uniformly distributed over the area of the entire GoF. To answer the question of the exact origin of this phosphorus requires a thorough investigation of all other engaged processes, which is beyond the scope of the present study.

3.6 Further studies

3.6.1 More complex model structures and geometries

The model will be further developed by incorporating more discrete subsystems for small local coastal areas linked with a great deep water central sea area still in the GoF. Efforts will be made to have more vertical layers as well. The shift to a full 3D system is not yet envisaged due to higher computational constraints.

3.6.2 Application to other study areas

In the frame of the Seabed project mentioned in the introduction, the models described in this study will be implemented on a finer scale for management support on the north coast of the GoF, in the Åbo sea area and in the Åland and Stockholm archipelagos.

4 Conclusions

4.1 Triggering anoxia

- A carbon-based model with explicit cycles for carbon, nitrogen and phosphorus is more capable of capturing dynamic features whereas, an implicit oxygen-based model is more efficient in long term average.
- The redox-sensitive sediment processes conditioned by a critical point, are formulated in the carbon-based model in a simple and effective manner. Linking the anoxic switch to the decomposition of organic carbon instead of the oxygen concentration in near-bottom water is a versatile approach. In fact it can simulate sediment nutrient fluxes under anaerobic condition although the water is well oxygenated, which has been observed.
- The carbon-based model is more robust while the oxygen-based model is sensitive to the critical oxygen threshold. Hence, it can be more applicable in a basin-wide scale in the Baltic Sea with a lesser need for in situ measurements of CO_2 fluxes.

4.2 Internal sources

- A potential infinite source of Phosphorus in the sediments is essential to maintain nutrient concentrations in the water column and subsequently to stabilize algal populations.

4.3 Flow dynamics

- An underlying daily hydrodynamics is a prerequisite to stabilize model simulations. The flow description must be able to undergo rapid variations to capture short duration mixing occurrences.

The carbon-based model will be developed by incorporating more distinct sub-systems and vertical layers and implemented on a basin-wide scale for management purpose on the northern coast of the GoF, in the Åbo sea area and in the Åland and Stockholm archipelagos.

REFERENCES

Alenius, P., Myrberg, K. & Nekrasov, A. (1998). The physical oceanography of the Gulf of Finland: a review. *Boreal Environment Research*, 3(2):97–125.

Ansari, A. (2010). *Eutrophication: causes, consequences and control*. Springer Verlag, 394 pp.

Bianchi, T., Engelhaupt, E., Westman, P., Andren, T., Rolff, C. & Elmgren, R. (2000). Cyanobacterial blooms in the Baltic Sea: Natural or human-induced? *Limnology and Oceanography*, 45(3):716–726.

Cerco, C. & Cole, T. (1994). Three-dimensional eutrophication model of Chesapeake Bay: Volume 1. Technical report, main report. Technical Report EL-94-4, US Army Engineer Waterways Experiment Station, Vicksburg, MS, 661 pp.

Dokulil, M. & Teubner, K. (2011). Eutrophication and Climate Change: Present Situation and Future Scenarios. *In: Eutrophication: causes, consequences and control*, pp. 1–16.

Döös, K., Meier, H. & Döscher, R. (2004). The Baltic haline conveyor belt or the overturning circulation and mixing in the Baltic. *Ambio*, 33(4):261–266.

Engqvist, A. & Andrejev, O. (2003). Water exchange of the Stockholm archipelago–a cascade framework modelling approach. *Journal of sea research*, 49(4):275–294.

Fonselius, S. (1969). Hydrography of the Baltic deep basins III. Fishery board of Sweden, Series hydrography, 97 pp. Technical report.

Frisk, T. (1982). An oxygen model for Lake Haukivesi. *Hydrobiologia*, 86(1):133–139.

Garber, J. (1984). Laboratory study of nitrogen and phosphorus remineralization during the decomposition of coastal plankton and seston. *Estuarine, Coastal and Shelf Science*, 18(6):685–702.

Heiskanen, A. & Tallberg, P. (1999). Sedimentation and particulate nutrient dynamics along a coastal gradient from a fjord-like bay to the open sea. *Hydrobiologia*, 393:127–140.

HELCOM (2002). Environment of the Baltic Sea Area 1994-1998. Technical report.

HELCOM (2004). The fourth Baltic Sea pollution load compilation (PLC-4). Technical report.

Kiirikki, M., Inkala, A., Kuosa, H., Pitkänen, H., Kuusisto, M. & Sarkkula, J. (2001). Evaluating the effects of nutrient load reductions on the biomass of toxic nitrogen-fixing cyanobacteria in the Gulf of Finland, Baltic Sea. *Boreal environment research*, 6(2):131–146.

Kiirikki, M., Lehtoranta, J., Inkala, A., Pitkanen, H., Hietanen, S., Hall, P., Tengberg, A., Koponen, J. & Sarkkula, J. (2006). A simple sediment process description suitable for 3D-ecosystem modelling–Development and testing in the Gulf of Finland. *Journal of Marine Systems*, 61(1-2):55–66.

Koponen, J., Alasaarela, E., Lehtinen, K., Sarkkula, J., Simbierowicz, P., Vepsä, H. & Virtanen, M. (1992). *Modelling the dynamics of a large sea area*. National Board of Waters and the Environment, Finland, 91 pp.

Kristensen, E., Ahmed, S. & Devol, A. (1995). Aerobic and anaerobic decomposition of organic matter in marine sediment: Which is fastest? *Limnology and Oceanography*, 40(8):1430–1437.

Kuusisto, M., Koponen, J. & Sarkkula, J. (1998). Modelled phytoplankton dynamics in the Gulf of Finland. *Environmental Modelling and Software*, 13(5-6):461–470.

Neumann, T. (2000). Towards a 3D-ecosystem model of the Baltic Sea. *Journal of Marine Systems*, 25(3-4):405–419.

Neumann, T., Fennel, W. & Kremp, C. (2002). Experimental simulations with an ecosystem model of the Baltic Sea: A nutrient load reduction experiment. *Global Biogeochemical Cycles*, 16(3):7–26.

Neumann, T. & Schernewski, G. (2008). Eutrophication in the Baltic Sea and shifts in nitrogen fixation analyzed with a 3D ecosystem model. *Journal of Marine Systems*, 74(1-2):592–602.

OECD (1982). *Eutrophication of Waters: Monitoring, Assessment and Control. OECD, Paris*. 154 pp.

Pett, R. (1989). Kinetics of microbial mineralization of organic carbon from detrital Skeletonema costatum cells. *Marine ecology progress series. Oldendorf*, 52(2):123–128.

Redfield, A. (1958). The biological control of chemical factors in the environment. *American Scientist*, 46(3):205–221.

Reissmann, J., Burchard, H., Feistel, R., Hagen, E., Lass, H., Mohrholz, V., Nausch, G., Umlauf, L. & Wieczorek, G. (2009). State-of-the-art review on vertical mixing in the Baltic Sea and consequences for eutrophication. *Progress in Oceanography*, 82:47–80.

Savchuk, O. (2000). Studies of the assimilation capacity and effects of nutrient load reductions in the eastern Gulf of Finland with a biogeochemical model. *Boreal environment research*, 5(2):147–163.

Schiewer, U. (2008). *Ecology of Baltic coastal waters*. Springer Verlag, 430 pp.

Seibert, J. (1997). Estimation of parameter uncertainty in the HBV model. *Nordic Hydrology*, 28(4):247–262.

Smith, V. (2003). Eutrophication of freshwater and coastal marine ecosystems a global problem. *Environmental Science and Pollution Research*, 10(2):126–139.

Smith, V. & Schindler, D. (2009). Eutrophication science: where do we go from here? *Trends in ecology & evolution*, 24(4):201–207.

Stigebrandt, A. & Wulff, F. (1987). A model for the dynamics of nutrients and oxygen in the Baltic proper. *Journal of Marine Research*, 45(3):729–759.

Thornton, J., Rast, W., Holland, M., Jolankai, G. & Ryding, S. (1999). *Assessment and control of nonpoint source pollution of aquatic ecosystems: a practical approach.* Parthenon Publishing Group, 466 pp.

Tyrrell, T. (1999). The relative influences of nitrogen and phosphorus on oceanic primary production. *Nature*, 400(6744):525–531.

Virtanen, M., Koponen, J., Dahlbo, K. & Sarkkula, J. (1986). Three-dimensional water-quality-transport model compared with field observations. *Ecological modelling*, 31(1-4):185–199.

Virtasalo, J. & Kotilainen, A. (2008). Phosphorus forms and reactive iron in late glacial, postglacial and brackish-water sediments of the Archipelago Sea, northern Baltic Sea. *Marine Geology*, 252(1-2):1–12.

OTHER REFERENCES

POM, Princeton Ocean Model (2011), homepage: `http://www.aos.princeton.edu/WWWPUBLIC/PROFS/NewPOMPage.html`

PVGIS, Photovoltaic Geographical Information System - Interactive Maps (2011), homepage: `http://re.jrc.ec.europa.eu/pvgis/apps4/pvest.php`

SMHI, HYdrological Predictions for the Environment - (HYPE) (2011), homepage: `http://balt-hypeweb.smhi.se/`

I ODE system adapted from Neumann et al.

I.1 Equations

$$\frac{\mathrm{d}C}{\mathrm{d}t} = (\mu_C - R_C).C + \frac{Q_{1B}^-}{V_1}.C + \frac{Q_{1B}^+}{V_1} Alg_{1B} \frac{C}{C+A}$$

$$\frac{\mathrm{d}A}{\mathrm{d}t} = (\mu_A - R_A).A + \frac{Q_{1B}^-}{V_1}.A + \frac{Q_{1B}^+}{V_1} Alg_{1B} \frac{A}{C+A}$$

$$\begin{aligned}\frac{\mathrm{d}A_{m1}}{\mathrm{d}t} = {} & \frac{1\,000}{N_{norm}} \left[\frac{-A_{m1}}{A_{m1}+N_{i1}} N_{inA} \frac{\mu_C.C+\mu_A.A}{h_1} \right] + L_{DA1}.D_1 - L_{AN1}.A_{m1} \\ & + \frac{Q_{12}^+}{V_1}.A_{m2} + \frac{Q_{12}^-}{V_1}.A_{m1} + \frac{Q_{1B}^-}{V_1}.A_{m1} + \frac{Q_{1B}^+}{V_1} \frac{NH_{4-1B}}{14.N_{norm}} + 0.3\frac{Q_{1F}}{V_1} c_{DINF}\end{aligned}$$

$$\begin{aligned}\frac{\mathrm{d}N_{i1}}{\mathrm{d}t} = {} & \frac{1\,000}{N_{norm}} \left[\frac{-N_{i1}}{A_{m1}+N_{i1}} N_{inA} \frac{\mu_C.C+\mu_A.A}{h_1} \right] - s_1.L_{DA1}.D_1.\theta(-O_{21}).\theta(N_{i1}) + L_{AN1}.A_{m1} \\ & + \frac{Q_{12}^+}{V_1}.N_{i2} + \frac{Q_{12}^-}{V_1}.N_{i1} + \frac{Q_{1B}^-}{V_1}.N_{i1} + \frac{Q_{1B}^+}{V_1} \frac{r_N.totN_{1B} - NH_{4-1B}}{14.N_{norm}} + 0.7\frac{Q_{1F}}{V_1} c_{DINF} + \dot{N}_{atm\ dep}\end{aligned}$$

$$\begin{aligned}\frac{\mathrm{d}PO_1}{\mathrm{d}t} = {} & \frac{1\,000}{P_{norm}} P_{inA} \frac{\mu_C.C+\mu_A.A}{h_1} + s_R.L_{DA1}.D_1 \\ & + \frac{Q_{12}^+}{V_1}.PO_2 + \frac{Q_{12}^-}{V_1}.PO_1 + \frac{Q_{1B}^-}{V_1}.PO_1 + \frac{Q_{1B}^+}{V_1} \frac{PO_{4-1B}}{31.P_{norm}} + \frac{Q_{1F}}{V_1} c_{DIPF}\end{aligned}$$

$$\begin{aligned}\frac{\mathrm{d}D_1}{\mathrm{d}t} = {} & \frac{1\,000}{N_{norm}} N_{inA} \frac{R_C.C+R_A.A}{h_1} - L_{DA1}.D_1 - \frac{l_{DS}}{h_1} D_1 \\ & + \frac{Q_{12}^+}{V_1}.D_2 + \frac{Q_{12}^-}{V_1}.D_1 + \frac{Q_{1B}^-}{V_1}.D_1\end{aligned}$$

$$\begin{aligned}\frac{\mathrm{d}O_{21}}{\mathrm{d}t} = {} & \frac{N_{norm}}{O_{norm}} \left[\frac{s_2.A_{m1}+s_3.N_{i1}}{A_{m1}+N_{i1}} \frac{1\,000}{N_{norm}} N_{inA} \frac{\mu_C.C+\mu_A.A}{h_1} \right] \\ & \frac{N_{norm}}{O_{norm}} \left[-s_4.L_{AN1}.A_{m1} - s_2 \left[\theta(O_{21}) + \theta(-O_{21})\theta(-N_{i1}) \right] L_{DA1}.D_1 \right] \\ & + \frac{Q_{12}^+}{V_1}.O_{22} + \frac{Q_{12}^-}{V_1}.O_{21} + \frac{Q_{1B}^-}{V_1}.O_{21} + \frac{Q_{1B}^+}{V_1} \frac{O_{21B}}{32.O_{norm}} + \dot{O}_{2\ atm\ dissol}\end{aligned}$$

$$\begin{aligned}\frac{\mathrm{d}A_{m2}}{\mathrm{d}t} = {} & L_{DA2}.D_2 - L_{AN2}.A_{m2} + \frac{r_{sed}}{h_2}.S \\ & - \frac{Q_{12}^+}{V_2}.A_{m2} - \frac{Q_{12}^-}{V_2}.A_{m1} + \frac{Q_{2B}^-}{V_2}.A_{m2} + \frac{Q_{2B}^+}{V_2} \frac{NH_{4-2B}}{14.N_{norm}}\end{aligned}$$

$$\begin{aligned}\frac{\mathrm{d}N_{i2}}{\mathrm{d}t} = {} & -s_1.L_{DA2}.D_2.\theta(-O_{22}).\theta(N_{i2}) + L_{AN2}.A_{m2} - s_1.\frac{r_{sed}}{h_2} S.\theta(-O_{22}).\theta(N_{i2}) \\ & - \frac{Q_{12}^+}{V_2}.N_{i2} - \frac{Q_{12}^-}{V_2}.N_{i1} + \frac{Q_{2B}^-}{V_2}.N_{i2} + \frac{Q_{2B}^+}{V_2} \frac{r_N.totN_{2B} - NH_{4-2B}}{14.N_{norm}}\end{aligned}$$

$$\begin{aligned}\frac{\mathrm{d}PO_2}{\mathrm{d}t} = {} & s_R.L_{DA2}.D_2 + s_R.\frac{r_{sed}}{h_2}(1-F_r)S + \frac{l_i}{h_2} I_P \\ & - \frac{Q_{12}^+}{V_2}.PO_2 - \frac{Q_{12}^-}{V_2}.PO_1 + \frac{Q_{2B}^-}{V_2}.PO_2 + \frac{Q_{2B}^+}{V_2} \frac{PO_{4-2B}}{31.P_{norm}}\end{aligned}$$

$$\begin{aligned}\frac{\mathrm{d}D_2}{\mathrm{d}t} = {} & -L_{DA2}.D_2 + \frac{l_{DS}}{h_1} D_1 - \frac{l_{DS}}{h_2} D_2 \\ & - \frac{Q_{12}^+}{V_2}.D_2 - \frac{Q_{12}^-}{V_2}.D_1 + \frac{Q_{2B}^-}{V_2}.D_2\end{aligned}$$

$$\begin{aligned}\frac{\mathrm{d}O_{22}}{\mathrm{d}t} = {} & \frac{N_{norm}}{O_{norm}} \left[-s_4.L_{AN2}.A_{m2} \left[\theta(O_{22}) + \theta(-O_{22})\theta(-N_{i2}) \right] \left(-s_2.L_{DA2}.D_2 + -s_2.\frac{r_{sed}}{h_2} S - s_4 \frac{r_{sed}}{h_2} S \right) \right] \\ & - \frac{Q_{12}^+}{V_2}.O_{22} - \frac{Q_{12}^-}{V_2}.O_{21} + \frac{Q_{2B}^-}{V_2}.O_{22} + \frac{Q_{2B}^+}{V_2} \frac{O_{22B}}{32.O_{norm}}\end{aligned}$$

$$\frac{\mathrm{d}S}{\mathrm{d}t} = -r_{sed}.S - L_{S-denit}.S + l_{DS}.D_2 - \tau.S$$

$$\frac{\mathrm{d}I_P}{\mathrm{d}t} = -l_i.I_P + s_R.r_{sed}.F_r.S - \tau.I_P$$

I.2 Functions

$Y(X_0, X) = \frac{X^2}{X^2+X_0^2}$

$\theta(N_i) = \begin{cases} 1. \text{ when } N_i \geq 0. \\ 0. \text{ when } N_i < 0. \end{cases}$

$\theta(O_2) = \begin{cases} 1. \text{ when } O_2 \geq O_{2T} \\ 0. \text{ when } O_2 < O_{2T} \end{cases}$

$\theta(-O_2) = \begin{cases} 1. \text{ when } O_2 \leq O_{2T} \\ 0. \text{ when } O_2 > O_{2T} \end{cases}$

Let X stand for C, cyanobacteria or A, other algae:

$\mu_X = \mu_{Xmax} . \frac{14(A_{m1}+N_{i1})N_{norm}}{14(A_{m1}+N_{i1})N_{norm}+K_{NX}} . \frac{31.PO_1.P_{norm}}{31.PO_1.P_{norm}+K_{PX}} . \frac{Ice.I}{Ice.I+K_{IX}} . f_{XT\mu} . f_{AC}$

$f_{XT\mu} = \exp(\int_{T_{opt\mu X}}^{T} \ln(\Theta) \mathrm{d}T)$

where $\Theta = a_{T\mu} + (1 - a_{T\mu}) \frac{T}{T_{opt\mu X}}$

$f_{AC} = 1 - \frac{c_A+c_C}{A_{max}}$

$R_X = R_{Xmax} . f_{XTR} . \frac{c_X - X_{min}}{c_X}$

$f_{XTR} = \exp(\int_{T_{optRX}}^{T} \ln(\Theta) \mathrm{d}T)$

where $\Theta = a_{TR} + (1 - a_{TR}) \frac{T}{T_{optRX}}$

$L_{DA1} = l_{DA} . (1 + \beta_{DA} . Y(T_{DA}, T_1))$

$L_{DA2} = l_{DA} . (1 + \beta_{DA} . Y(T_{DA}, T_2))$

$L_{AN1} = \theta(O_{21}) \frac{O_{21}}{O_{21}+O_{AN}} l_{AN} \exp(\beta_{AN} T_1)$

$L_{AN2} = \theta(O_{22}) \frac{O_{22}}{O_{22}+O_{AN}} l_{AN} \exp(\beta_{AN} T_2)$

$r_{sed} = r_{sed0} . \exp(\beta_{sed} . T_2)$

$F_r = F_{r0} . \theta(O_{22})$

$l_i = l_{i0} . \theta(-O_{22})$

$L_{S-denit} = \theta(O_2) . r_{sed}$

$\dot{O}_{2\ atm\ dissol} = p_{vel}(O_{sat} - O_{21})$

where $O_{sat} = \frac{a_0}{O_{norm}}(a_1 + a_2 . T_1)$

I.3 Parameters

$A_{min} = 0.01\ g/m^2$	$l_{AN} = 0.1\ d^{-1}$	$s_R = 1/16$
$A_{max} = 300\ g/m^2$	$l_{DA} = 0.003\ d^{-1}$	$TDA = 13\ ^\circ C$
$a_0 = 31.25\ mmol/m^3$	$l_{DS} = 3.5\ m/d$	$T_{opt\mu C} = 25\ ^\circ C$
$a_1 = 14.603$	$l_{i0} = 0.1\ d^{-1}$	$T_{opt\mu A} = 15\ ^\circ C$
$a_2 = 0.4025\ ^\circ C^{-1}$	$N_{inA} = 0.0193/14.$	$T_{optR} = 25\ ^\circ C$
$a_{T\mu C} = 1.14$	$N_{norm} = 4.5\ mmol/m^3$	$V = 1.1\ 10^{12}\ m^3$
$a_{T\mu A} = 1.001$	$O_{AN} = 0.01$	$V_1 = h_1/38 * V$
$a_{TR} = 1.05$	$O_{norm} = 375\ mmol/m^3$	$V_2 = h_2/38 * V$
$C_{min} = 0.5\ g/m^2$	$O_{2T} = 8.5\ g/m^3$	$\beta_{AN} = 0.11\ ^\circ C^{-1}$
$c_{DINF} = 1053.7\ mg/m^3$	$P_{inA} = 0.00268/31.$	$\beta_{DA} = 20\ ^\circ C^{-1}$
$c_{DIPF} = 61.468\ mg/m^3$	$P_{norm} = N_{norm} * s_R$	$\beta_{sed} = 0.175\ ^\circ C^{-1}$
$f_{r0} = 0.18$	$p_{vel} = 5\ m/d$	$\mu_{Cmax} = 0.5\ d^{-1}$
$h_1 = 20\ m$	$R_{Cmax} = 0.1\ d^{-1}$	$\mu_{Amax} = 0.7\ d^{-1}$
$h_2 = 18\ m$	$R_{Amax} = 0.15\ d^{-1}$	$\tau = 0.0001\ d^{-1}$
$K_{NC} = 0\ mg/m^3$	$r_{sed0} = 0.002\ d^{-1}$	

$K_{PC} = 2\ mg/m^3$	$r_N = 0.5$
$K_{NA} = 7\ mg/m^3$	$s_1 = 5.3$
$K_{PA} = 1\ mg/m^3$	$s_2 = 6.625$
$K_{IC} = 20\ MJ/m^2/d$	$s_3 = 8.125$
$K_{IA} = 15\ MJ/m^2/d$	$s_4 = 2/3$

II ODE system adapted from Kiirikki et al.

II.1 Equations

$$\frac{\mathrm{d}C}{\mathrm{d}t} = (\mu_C - R_C).C + \frac{Q_{1B}^-}{V_1}.C + \frac{Q_{1B}^+}{V_1} Alg_{1B} \frac{C}{C+A}$$

$$\frac{\mathrm{d}A}{\mathrm{d}t} = (\mu_A - R_A).A + \frac{Q_{1B}^-}{V_1}.A + \frac{Q_{1B}^+}{V_1} Alg_{1B} \frac{A}{C+A}$$

$$\begin{aligned}\frac{\mathrm{d}c_{DIN1}}{\mathrm{d}t} &= \beta_1.c_{Ndet1} - 1\,000(\mu_A.A + \mu_C.C)\frac{N_{inA}}{h_1} \\ &+ \frac{Q_{12}^+}{V_1}.c_{DIN2} + \frac{Q_{12}^-}{V_1}.c_{DIN1} + \frac{Q_{1B}^-}{V_1}.c_{DIN1} + \frac{Q_{1B}^+}{V_1} r_N.totN_{1B} + \frac{Q_{1F}}{V_1} c_{DINF} + \dot{N}_{atm\ dep}\end{aligned}$$

$$\begin{aligned}\frac{\mathrm{d}c_{DIP1}}{\mathrm{d}t} &= \gamma_1.c_{Pdet1} - 1\,000(\mu_A.A + \mu_C.C)\frac{P_{inA}}{h_1} \\ &+ \frac{Q_{12}^+}{V_1}.c_{DIP2} + \frac{Q_{12}^-}{V_1}.c_{DIP1} + \frac{Q_{1B}^-}{V_1}.c_{DIP1} + \frac{Q_{1B}^+}{V_1} PO_{4-1B} + \frac{Q_{1F}}{V_1} c_{DIPF}\end{aligned}$$

$$\begin{aligned}\frac{\mathrm{d}c_{Ndet1}}{\mathrm{d}t} &= 1\,000 * N_{inA}\frac{R_C.C+R_A.A}{h_1} - \beta_1.c_{Ndet1} - \frac{s}{h_1} c_{Ndet1} \\ &+ \frac{Q_{12}^+}{V_1}.c_{Ndet2} + \frac{Q_{12}^-}{V_1}.c_{Ndet1} + \frac{Q_{1B}^-}{V_1}.c_{Ndet1}\end{aligned}$$

$$\begin{aligned}\frac{\mathrm{d}c_{Pdet1}}{\mathrm{d}t} &= 1\,000 * P_{inA}\frac{R_C.C+R_A.A}{h_1} - \gamma_1.c_{Pdet1} - \frac{s}{h_1} c_{Pdet1} \\ &+ \frac{Q_{12}^+}{V_1}.c_{Pdet2} + \frac{Q_{12}^-}{V_1}.c_{Pdet1} + \frac{Q_{1B}^-}{V_1}.c_{Pdet1}\end{aligned}$$

$$\begin{aligned}\frac{\mathrm{d}c_{Cdet1}}{\mathrm{d}t} &= 1\,000 * C_{inA}\frac{R_C.C+R_A.A}{h_1} - \frac{s}{h_1} c_{Cdet1} \\ &+ \frac{Q_{12}^+}{V_1}.c_{Cdet2} + \frac{Q_{12}^-}{V_1}.c_{Cdet1} + \frac{Q_{1B}^-}{V_1}.c_{Cdet1}\end{aligned}$$

$$\begin{aligned}\frac{\mathrm{d}c_{DIN2}}{\mathrm{d}t} &= \beta_2.c_{Ndet2} + \mu\frac{1-fr_{dn}}{h_2}.N_V \\ &- \frac{Q_{12}^+}{V_2}.c_{DIN2} - \frac{Q_{12}^-}{V_2}.c_{DIN1} + \frac{Q_{2B}^-}{V_2}.c_{DIN2} + \frac{Q_{2B}^+}{V_2} r_N.totN_{2B}\end{aligned}$$

$$\begin{aligned}\frac{\mathrm{d}c_{DIP2}}{\mathrm{d}t} &= \gamma_2.c_{Ndet2} + \mu\frac{1-fr_P+\gamma_{Pin}}{h_2} P_V \\ &- \frac{Q_{12}^+}{V_2}.c_{DIP2} - \frac{Q_{12}^-}{V_2}.c_{DIP1} + \frac{Q_{2B}^-}{V_2}.c_{DIP2} + \frac{Q_{2B}^+}{V_2} PO_{4-2B}\end{aligned}$$

$$\begin{aligned}\frac{\mathrm{d}c_{Ndet2}}{\mathrm{d}t} &= -\beta_2.c_{Ndet2} + \frac{s}{h_1} c_{Ndet1} - \frac{s}{h_2} c_{Ndet2} \\ &- \frac{Q_{12}^+}{V_2}.c_{Ndet2} - \frac{Q_{12}^-}{V_2}.c_{Ndet1} + \frac{Q_{2B}^-}{V_2}.c_{Ndet2}\end{aligned}$$

$$\begin{aligned}\frac{\mathrm{d}c_{Pdet2}}{\mathrm{d}t} &= -\gamma_2.c_{Pdet2} + \frac{s}{h_1} c_{Pdet1} - \frac{s}{h_2} c_{Pdet2} \\ &- \frac{Q_{12}^+}{V_2}.c_{Pdet2} - \frac{Q_{12}^-}{V_2}.c_{Pdet1} + \frac{Q_{2B}^-}{V_2}.c_{Pdet2}\end{aligned}$$

$$\begin{aligned}\frac{\mathrm{d}c_{Cdet2}}{\mathrm{d}t} &= \frac{s}{h_1} c_{Cdet1} - \frac{s}{h_2} c_{Cdet2} \\ &- \frac{Q_{12}^+}{V_2}.c_{Cdet2} - \frac{Q_{12}^-}{V_2}.c_{Cdet1} + \frac{Q_{2B}^-}{V_2}.c_{Cdet2}\end{aligned}$$

$$\frac{\mathrm{d}N_V}{\mathrm{d}t} = -\mu.N_V - \tau.N_V + s.c_{Ndet2}$$

$$\frac{\mathrm{d}P_V}{\mathrm{d}t} = -\mu.P_V + s.c_{Pdet2}$$

$$\frac{\mathrm{d}C_V}{\mathrm{d}t} = -\mu.C_V - \tau.C_V + s.c_{Cdet2}$$

$$\frac{\mathrm{d}P_{FeV}}{\mathrm{d}t} = \mu.(fr_P - \gamma_{Pin})P_V - \tau.P_{FeV}$$

II.2 Functions

Let X stand for C, cyanobacteria or A, other algae:

$\mu_X = \mu_{Xmax} \cdot \frac{c_{DIN1}}{c_{DIN1}+K_{NX}} \cdot \frac{c_{DIP1}}{c_{DIP1}+K_{PX}} \cdot \frac{Ice.I}{Ice.I+K_{IX}} \cdot f_{XT\mu} \cdot f_{AC}$

$f_{XT\mu} = \exp(\int_{T_{opt\mu X}}^{T} \ln(\Theta) \mathrm{d}T)$

where $\Theta = a_{T\mu} + (1 - a_{T\mu}) \frac{T}{T_{opt\mu X}}$

$f_{AC} = 1 - \frac{c_A + c_C}{A_{max}}$

$R_X = R_{Xmax} . f_{XTR} . \frac{c_X - X_{min}}{c_X}$

$f_{XTR} = \exp(\int_{T_{optRX}}^{T} \ln(\Theta) \mathrm{d}T)$

where $\Theta = a_{TR} + (1 - a_{TR}) \frac{T}{T_{optRX}}$

$\beta_{1,2} = \beta_0 . f_{T\beta}(T_{1,2})$

$f_{T\beta} = \exp(\int_{T_{opt\beta}}^{T} \ln(\Theta) \mathrm{d}T)$

where $\Theta = a_{T\beta} + (1 - a_{T\beta}) \frac{T}{T_{opt\beta}}$

$\gamma_{1,2} = \gamma_0 . f_{T\gamma}(T_{1,2})$

$f_{T\gamma} = \exp(\int_{T_{opt\gamma}}^{T} \ln(\Theta) \mathrm{d}T)$

where $\Theta = a_{T\gamma} + (1 - a_{T\gamma}) \frac{T}{T_{opt\gamma}}$

$\mu = \mu_{max} . f_{T\mu}(T)$

$f_{T\mu} = \exp(\int_{T_{opt\mu}}^{T} \ln(\Theta) \mathrm{d}T)$

where $\Theta = a_{T\mu} + (1 - a_{T\mu}) \frac{T}{T_{opt\mu}}$

$$fr_{dn} = fr_P = \begin{cases} 0.7 \text{ when } \mu.C_V < C_{Cr} \\ 0. \text{ when } \mu.C_V > C_{Cr} \end{cases}$$

$$\gamma_{pin} = \begin{cases} 0. \text{ when } \mu.C_V < C_{Cr} \\ 3.75 \text{ when } \mu.C_V > C_{Cr} \end{cases}$$

II.3 Parameters

$A_{min} = 0.01\ g/m^2$	$h_2 = 18\ m$	$T_{opt\mu A} = 15\ °C$
$A_{max} = 300\ g/m^2$	$K_{NC} = 0\ mg/m^3$	$T_{optR} = 25\ °C$
$a_{T\mu C} = 1.14$	$K_{PC} = 2\ mg/m^3$	$T_{opt\beta} = 18\ °C$
$a_{T\mu A} = 1.001$	$K_{NA} = 7\ mg/m^3$	$T_{opt\gamma} = 18\ °C$
$a_{TR} = 1.05$	$K_{PA} = 1\ mg/m^3$	$T_{opt\mu} = 18\ °C$
$a_\beta = 1.31$	$K_{IC} = 20\ MJ/m^2/d$	$V = 1.1\ 10^{12}\ m^3$
$a_\gamma = 1.6$	$K_{IA} = 15\ MJ/m^2/d$	$V_1 = h_1/38 * V$
$a_\mu = 1.3$	$N_{inA} = 0.0193/14.$	$V_2 = h_2/38 * V$
$C_{min} = 0.5\ g/m^2$	$P_{inA} = 0.00268/31.$	$\beta_0 = 0.018\ d^{-1}$
$c_{DINF} = 1053.7\ mg/m^3$	$R_{Cmax} = 0.1\ d^{-1}$	$\gamma_0 = 0.043\ d^{-1}$
$c_{DIPF} = 61.468\ mg/m^3$	$R_{Amax} = 0.15\ d^{-1}$	$\mu_{Cmax} = 0.5\ d^{-1}$
$C_{cr} = 240\ mg\ C/m^2/d$	$r_N = 0.5$	$\mu_{Amax} = 0.7\ d^{-1}$
$C_{inA} = 41 * P_{inA}$	$s = 1.0\ m/d$	$\mu_{Amax} = 0.7\ d^{-1}$
$h_1 = 20\ m$	$T_{opt\mu C} = 25\ °C$	$\tau = 0.0001\ d^{-1}$

III GEMSS output: Text files' organization

There are 3 text files needed to recover 1 simulation:

- a file with a .hdm extension
- a file with a .grd extension
- a file with a .ctm extension.

III.1 The HDM file

This file starts by stating generic information on the current simulation.
For example:

```
$GLLVHTModelResults
$Data for GLLVHT Post Processor
$File name path = C:\GEMSS
$26-Apr-11
$Scenario Name:  C:\GEMSS\Apps\BalticSea\Output\Scenario_2004S1_Wave
```

It then gives the number and the names (and unit if there is one) of the extra variables recorded for this simulation (the 3 components of the velocity vector are not mentioned but they are implicitly considered to be the first 3 variables).

For example:

```
7
Temperature C
Conc.  of Salinity ppt
Cell Evap.  Rate m3̂/sec
Cell Evap.  Volume m3̂
Wave Height m
Wave Period secs
Wave Modified Chezy
```

The last part of the HDM file consists of the date of the recorded data. It first gives the number of time steps and the lists the time steps by associating a time index (first column) and a Julian day (second column), for example (the last columns' signification does not involve the physics):

```
184
1, 37987.345833, 3
2, 37989.333333, 3
3, 37991.340972, 3
4, 37993.337500, 3
5, 37995.334028, 3
6, 37997.342361, 3
7, 37999.343056, 3
8, 38001.343056, 3
9, 38003.343056, 3
10, 38005.333333, 3
...
184, 38352.334028, 3
```

III.2 The GRD file

This file will give the specifications of the grid. The first line gives the maximum values for each spatial index, in order in the following example, maximum number of cells in the west-east direction (referred as imax), maximum number of cells in the south-north direction (referred as jmax) and maximum number of vertical cells (referred as kmax) (the last 3 numbers I don't know about):

```
104, 134, 46, 4110, 5381, 1
```

The following lines give the vertical griding.
The second line of the file gives the height (in meters) of the upper layer's top and the lower layer's bottom (The following zeros do not carry physical meaning here):

```
0.140000E+02,-0.243000E+03, 0.000000E+00, 0.000000E+00, 0.000000E+00,
0.000000E+00
```

The following lines give each vertical layer's specifications: vertical index, vertical thickness of the layer and height of the top of the layer (same remark far the final zeros):

```
1, 0.700000E+01, 0.140000E+02, 0.000000E+00, 0.000000E+00, 0.000000E+00
2, 0.700000E+01, 0.700000E+01, 0.000000E+00, 0.000000E+00, 0.000000E+00
3, 0.400000E+01, 0.000000E+00, 0.000000E+00, 0.000000E+00, 0.000000E+00
4, 0.400000E+01,-0.400000E+01, 0.000000E+00, 0.000000E+00, 0.000000E+00
...
46, 0.800000E+01,-0.235000E+03, 0.000000E+00, 0.000000E+00, 0.000000E+00
```

The next portion of the file gives the coordinates of the each useful pair of horizontal indices (i,j). A single lines give in order: i, j, west-east coordinate, south-north coordinates, (and two zeros) like this:

```
1, 1, 4499747.0000, 3485088.0000, 0.0000, 0.0000
2, 1, 4510881.5000, 3482112.5000, 0.0000, 0.0000
3, 1, 4520990.0000, 3476676.5000, 0.0000, 0.0000
4, 1, 4529054.0000, 3468446.7500, 0.0000, 0.0000
5, 1, 4537682.0000, 3460807.0000, 0.0000, 0.0000
...
50, 135, 5114343.0000, 4798098.0000, 0.0000, 0.0000
```

The file goes on there but the rest is redundant.

III.3 The CTM file

This file contains the simulated data. One single line contains data for one node at one specific time. It states in order: the time index, the i index, the j index, the k index, a number I don't know about, u, v, w (the 3 components of the velocity vector in cm/s), the other variables according to the order given in the HDM file.

For example:

```
24,75,63,4,-0.400000E+01, 0.451042E+01,-0.276508E+01,-0.525706E-03,-0.151159E+01,
0.833279E+01, 0.738793E-01, 0.797897E+02, 0.288823E+00, 0.234702E+01,
0.400000E+02, 1
```